A new method of AC calorimetry using thermoelectric devices
by Gregory James Pastalan

A thesis submitted in partial fulfillment of the requirements for the degree of Master of Science in Physics
Montana State University

Abstract:
The field of calorimetry currently uses separate measurement methods for determining the thermal conductivity and heat capacity per unit volume of a material. This thesis describes the construction of a prototypes apparatus which gathers the data necessary to calculate both of these properties of a solid material. The novelty of this apparatus is that it uses thermoelectric devices in both the stimulating and receiving portions of its design for both dc and ac measurements, so that both thermal conductivity and heat capacity can be determined. The two materials studied at room temperature were Triglycine Fluoberyllate (TGFB), a ferroelectric crystal, and Lead. The data gathered from the apparatus were temperature values expressed as complex numbers representing amplitude and phase relative to the thermal input power. The measurements, for no sample and lead sample being measured showed good agreement with the theoretical prediction of the received signal having decreasing amplitude and increasing phase angle with respect to the driving signal over a frequency range of 0.5 to 15.0 Hz. The data from the TGFB sample showed good agreement with predicted behavior over the frequency range 0.5 to 3.0 Hz.

A NEW METHOD OF AC CALORIMETRY USING THERMOELECTRIC DEVICES

by

Gregory James Pastalan

A thesis submitted in partial fulfillment
of the requirements for the degree

of

Master of Science

in

Physics

MONTANA STATE UNIVERSITY
Bozeman, Montana

April 1994

APPROVAL

of a thesis submitted by

Gregory James Pastalan

This thesis has been read by each member of the thesis committee and has been found to be satisfactory regarding English usage, format, citations, bibliographic style, and consistency, and is ready for submission to the College of Graduate Studies.

May 5, 1994
Date

V. Hugo Schmidt
Chairman, Graduate Committee

Approved for the Major Department

5-5-94
Date

Head, Major Department

Approved for the College of Graduate Studies

5/11/94
Date

Graduate Dean

STATEMENT OF PERMISSION TO USE

In presenting this thesis in partial fulfillment of the requirements for a Master's degree at Montana State University, I agree that the Library shall make it available to borrowers under rules of the Library.

If I have indicated my intention to copyright this thesis by including a copyright notice page, copying is allowable only for scholarly purposes, consistent with "fair use" as prescribed in the U.S. Copyright Law. Requests for permission for extended quotation from or reproduction of this thesis in whole or in parts may be granted only by the copyright holder.

Signature Thyos J Pastel

Date May 5, 1994

ACKNOWLEDGMENTS

I wish to express my thanks and appreciation to all the people who helped make this thesis project a reality. My thanks to my thesis advisor Dr. V. Hugo Schmidt for his help, advice and most of all his patience for allowing me to work in his laboratory and complete a masters thesis. I also want to thank both Erik Andersen and Norm Williams for their timely technical advice and assistance during the various stages of the design, assembly and testing of the apparatus. My thanks to Bob Parker for his help in computer interfacing the data gathering equipment which significantly reduced the data acquisition time and enhanced its accuracy. Also I wish to thank Dan Teske for his advice and encouragement throughout the entire project.

Finally I wish to acknowledge some unsung teachers, namely Jan Pastalan, Tony Nizalowski, and Mario Lopez, who through the example of their lives, have taught me to be calm, to be strong, and to persevere.

TABLE OF CONTENTS

LIST OF TABLES

LIST OF FIGURES

LIST OF FIGURES-CONTINUED

ABSTRACT

The field of calorimetry currently uses separate measurement methods for determining the thermal conductivity and heat capacity per unit volume of a material. This thesis describes the construction of a prototype apparatus which gathers the data necessary to calculate both of these properties of a solid material. The novelty of this apparatus is that it uses thermoelectric devices in both the stimulating and receiving portions of its design for both dc and ac measurements, so that both thermal conductivity and heat capacity can be determined. The two materials studied at room temperature were Triglycine Fluoberyllate (TGFB), a ferroelectric crystal, and Lead. The data gathered from the apparatus were temperature values expressed as complex numbers representing amplitude and phase relative to the thermal input power. The measurements for no sample and lead sample being measured showed good agreement with the theoretical prediction of the received signal having decreasing amplitude and increasing phase angle with respect to the driving signal over a frequency range of 0.5 to 15.0 Hz. The data from the TGFB sample showed good agreement with predicted behavior over the frequency range 0.5 to 3.0 Hz.

CHAPTER 1

INTRODUCTION

This thesis reports the construction and successful operation of a prototype AC calorimetry apparatus for solid samples which makes use of thermoelectric devices to apply and receive temperature waves. This method allows calculation of thermal diffusivity, thermal conductivity, and specific heat of a solid material from the gathered data.

Definitions and Basic Theory

There are three fundamental thermodynamic properties which need to be defined, specific heat, thermal conductivity, and thermal diffusivity.

The heat capacity of a material at constant volume is defined to be $C_v = (dQ/dT)_v$. As the material is heated at constant volume in a reversible process, dQ is the amount of heat necessary to raise the temperature of the material by dT. When considering the properties of a unit mass of a material, the properties are called specific. Hence the definition of specific heat is the heat capacity at constant volume per unit mass of the material, $c_v = m^{-1} (dQ/dT)_v$.

Thermal conductivity is defined from Fourier's heat conduction law, $dQ/dt = - kA(dT/dx)$. In the rearranged expression $(dQ/dt)/A = J = -k(dT/dx)$, the thermal conductivity k of a material is the constant of proportionality relating the heat flux per unit area to the temperature gradient in the material.

The thermal diffusivity, defined as $\alpha = k/\rho c_v$, is the ratio of thermal conductivity to the product of density of the material and the specific heat at constant volume. More simply, it is the ratio of thermal conductivity to heat capacity per unit volume.

Thermal diffusivity determines how quickly a material responds when a temperature transient is applied to its surface.

To illustrate how the thermal diffusivity α enters into the one-dimensional ac heat flow process, consider a thin slab of thickness dx perpendicular to the heat flow direction x. From the Fouier law, the heat flux entering the left side is $-kA\partial T/\partial x$. The flux entering the right side is $+kA[\partial T/\partial x + (\partial^2 T/\partial x^2)dx]$. The net heat flux input $kAdx\partial^2 T/\partial x^2$ is equal to the heat capacity per unit volume $c_v\rho$ multiplied by the volume Adx of the slab and the rate of temperature change $\partial T/\partial t$, so we obtain the differential equation for time-dependent one-dimensional heat flow,

$$\partial T/\partial t = \alpha\partial^2 T/\partial x^2 \quad (1\text{-}1).$$

Measurement Methods

DC Methods

Since the thermal diffusivity has a known relation to heat capacity and thermal conductivity, knowledge of any two easily yields the third. In the case of heat capacity, there exist two methods for making dc measurements. The first method is to produce joule heating from a current-carrying resistor attached to the sample, then measure the temperature change of the sample by an attached thermometer.

The second method requires the sample to reach an elevated equilibrium temperature, usually through contact with a heat reservoir. It is then placed in contact with a heat sink, and the sample-heat-sink system is thermally isolated. The calorimeter (heat sink) can then be observed for change in its temperature or for a phase transition. Two common examples of these methods are the Nernst-Eucken, used in the liquid helium temperature range, and the Method of Mixtures, used for temperatures > 20 K.[1-3]

A common dc method of determining specific heat is through the use of a Differential Thermal Analyzer (DTA). The DTA compares the temperatures of two materials, the sample under study and a thermally inert reference sample as both samples are heated in a furnace at a constant rate. Inside each sample are thermocouple junctions connected by a common wire. When the sample undergoes an enothermic or exothermic

reaction heat energy is absorbed or liberated respectively. This results in a temperature difference between the sample and reference yielding a voltage difference between them. Hence as voltage is plotted as a function of time a voltage spike will appear at a temperature where a phase transition occurs.

AC Methods

An important contribution to the development of the theory of AC calorimetry was made by Sullivan and Seidel.[4,5] Heat energy is supplied sinusoidally to one end of a sample, to which the magnitude and phase of the temperature at the opposite end of the sample are compared. The usual boundary condition is that the sample is in contact with a thermal reservoir such that the sample can quickly return to thermal equilibrium once given an energy input.

There are several methods of generating an incident ac temperature wave upon a sample surface. One method uses a chopped laser beam incident on one face of the sample while thermocouples attached along the sample determine temperature as a function of position and time.[6,7]

Another method makes use of thermally conductive films which are deposited on opposite ends of a sample.[8] One face acts as a signal generator while the other acts as a receiver. A third method, which is similar to our method, makes use of a thermoelectric device to generate an ac temperature wave.[9] Santucci and Verdini[9] studied a sample of

copper at a pressure of 1 x 10^{-6} mbar, providing it an ac temperature wave from a Melcor FC-06-32-06 TL unit and measuring temperatures along the sample via thermocouples. A United States Patent[10] was granted in 1973 to Stanley and Reich for a method and apparatus for measuring thermal conductivity and thermoelectric properties of solids using thermoelectric devices. Their configuration of sandwiching a sample between two thermoelectric devices is identical to ours. However, the work of Stanley and Reich was limited to applying a dc voltage signal to the driver instead of an ac voltage signal.

CHAPTER 2

EXPERIMENTAL SETUP

The system to be described consists of several components, some of which were built in-house.

The basic idea of this method is to apply an ac temperature wave to a solid and compare the amplitude and phase shift of the transmitted signal to the applied signal. In the low frequency limit, results yield thermal conductivity, while in the high frequency limit, results yield thermal diffusivity from which one finds specific heat if the thermal conductivity is known.

A description of the overall system will be given first, followed by a more detailed description of the critical components.

The system makes use of a pair of thermoelectric devices, which sandwich the solid sample between them. One device is used in an active role, as a driver, while the second device is used in a passive mode, as a receiver. The driver converts an applied ac voltage into a temperature wave, which propagates through the solid under study. The receiver, on the opposite side of the solid, accepts the temperature wave and converts this signal into an ac voltage. The thermoelectric elements used are produced by MELCOR[11] and employ the Peltier[3] and Seebeck[3] effects in their

operation.

Through use of a lock-in amplifier the in-phase and quadrature components of the ac voltage from the receiver are compared with the ac voltage applied to the driver. The lock-in amplifier is necessary because the amplitude of the receiver output signals is very small.

The system can be divided into two parts, the probe and the external equipment, as seen in Figure 1. At the bottom of the probe is attached the copper slug which contains the thermoelectric elements and the samples.

The copper slug, shown in Figure 2, consists of a cylindrical copper mass which acts as a thermal reservoir upon which three pairs of Melcor devices are aligned parallel to the cylinder axis and spaced 120 degrees apart. The three Melcor pairs are arranged with one mounted on a fixed surface, while the second is mounted to a retractable block which is attached by a compression spring to the bottom of the copper slug. This design allows for the easy insertion and removal of solid samples.[12] A copper can attached by three screws to the bottom of the slug acts as a thermal shield covering the copper slug. The copper slug is connected to a thin-wall stainless steel tube, 1.47 m long and 2.5 cm diameter, by a Teflon cylinder which acts as an insulating mating surface. The tube length is determined by the dimensions of the dewar.

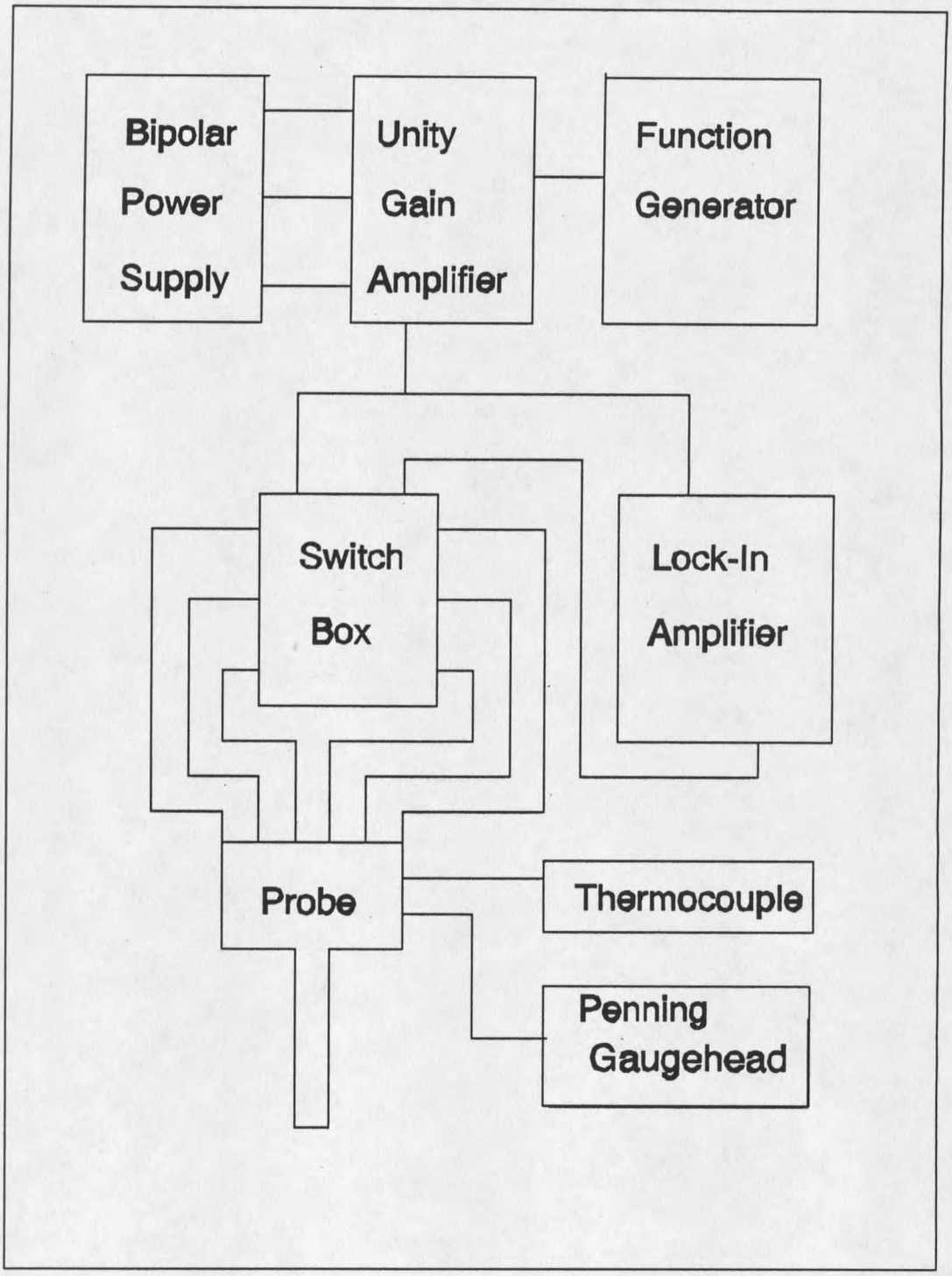

Overall System Schematic

Figure 1

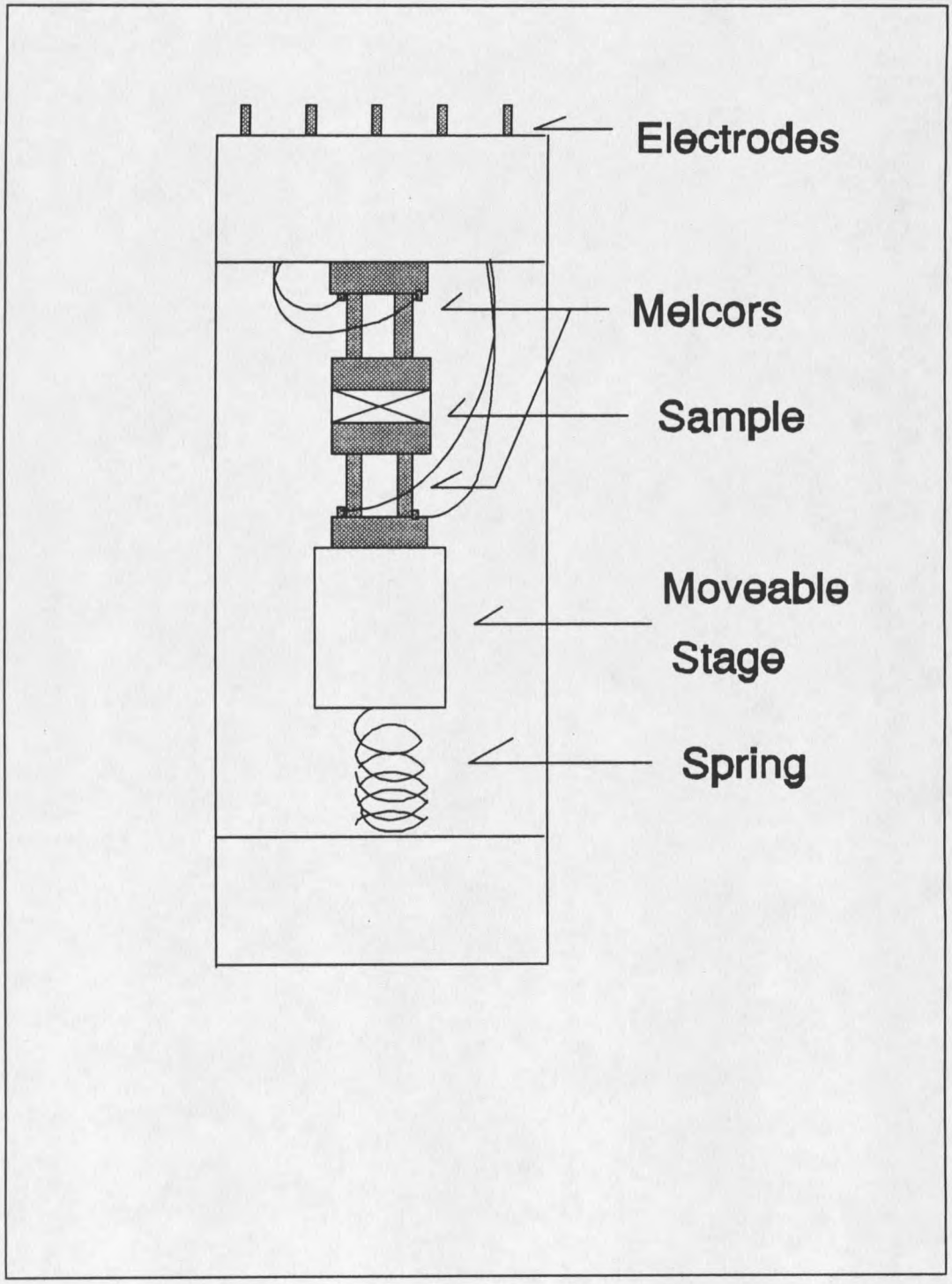

Copper Slug

Figure 2

The tube houses coaxial cable connections between the slug and the top flange.

These internal coaxial cables are connected to external coaxial cables by floating BNC connectors. Floating connectors are necessary since the driver and receiver signals must be isolated in order to avoid ground loop problems. The tube also contains leads to a chromel-alumel thermocouple which is attached to the copper slug in order to monitor the ambient temperature of the system.

The probe is connected electrically to a switch box which connects to any one of the three Melcor pairs at a given time. The switch box is divided into driver and receiver channels. The driver channel is connected to a unity gain amplifier which acts to impedance match the Hewlett-Packard 3325B Synthesizer/Function Generator to the low-impedance Melcor device. The output of the unity gain amplifier is also connected to the Reference Signal port of the EG&G 5204 Lock-In Amplifier. The receiver channel of the switch box is connected to the Signal-In port of the lock-in amplifier. The unity gain amplifier[13] and switch box were constructed in-house.

The probe is inserted into the dewar which is capable of achieving internal temperatures over the range +4 K to +375 K. The range of temperatures used in this project were +25°C to +80°C.

Critical Components of the System

The three critical components of the system are the thermoelectric elements, the Lock-In Amplifier and the thermocouple based mean temperature monitoring system.

Thermoelectric Elements

The thermoelectric elements used in this apparatus are manufactured by the MELCOR Corporation and will be referred to hereafter as the Melcors. These devices consist of two ceramic slabs which are composed of alumina (Al_2O_3) separated by eight semiconductor pillars (Bi_2Te_3) oriented orthogonal to the ceramic slabs as seen in Figure 3. The Peltier[3] effect takes place at the soldered junctions joining the pillars to the slabs. As shown in Figure 4 the semiconductor pillars are doped to be alternately n and p type.

The solder junction joining the n and p type materials is non-rectifing so that current flow is not impeded when an external voltage is applied.[11] As depicted in Figure 4, the negative thermal gradient and hence the flow of heat is in the same direction as the majority carrier flow in both types of semiconductor. This is the Peltier[3] effect which, for the applied voltage polarity shown, transports heat energy via the majority charge carriers from the upper slab to the lower slab. This mode of operation is denoted the "cooling" mode. Joule heating is produced in the

semiconductor, so the net cooling provided by the upper slab is that produced thermoelectrically, less the joule heat flow to the upper slab. When the applied voltage polarity is reversed, the net heat available at the upper slab includes contributions from both joule heating and thermoelectric heating. Hence this operation mode is denoted as the "heating" mode.[11]

The Peltier effect can be expressed mathematically[14]

$$j^q = \Pi j \quad (2\text{-}1)$$

where j^q is the thermal current while j is the electric current and the constant of proportionality Π, is the Peltier coefficient. The Peltier coefficient is related to the thermoelectric power by the relation[14] ,

$$\Pi = QT \quad (2\text{-}2)$$

with Q being the thermoelectric power or Seebeck coefficient, and T is temperature. The Seebeck coefficient is the constant of proportionality between the temperature gradient in the material and the resulting emf.

$$V = -\int \xi \cdot dl = Q\Delta T \quad (2\text{-}3)$$

Since the Melcors make use of both n and p type Bi_2Te_3, the best results that could be found were $|Q_n - Q_p| = (0.63K/mV)^{-1}$, which is discussed in chapter three. Likewise expression (2-2) becomes $|\Pi_n - \Pi_p| = |Q_n - Q_p|T$, so at T = 300K the expression becomes $|\Pi_n - \Pi_p| = 0.476V$.

If an ac current flows in the Melcor, the heating and cooling cycles alternate with the same frequency as the

applied ac voltage. This describes the action of the driver Melcor in the apparatus.

The receiver Melcor acts passively as a thermal transducer, receiving the temperature waves from the sample sandwiched between the two Melcors. Since the receiver Melcor is bounded on top by the sample and beneath by the copper slug a temperature gradient is created between the two alumina slabs. Because of this thermal gradient an electrical potential is developed due to the Seebeck effect.[3] In the case where the temperature gradient is constant the receiver Melcor will yield a dc voltage. When the temperature gradient is alternating the receiver Melcor yields an ac voltage response.

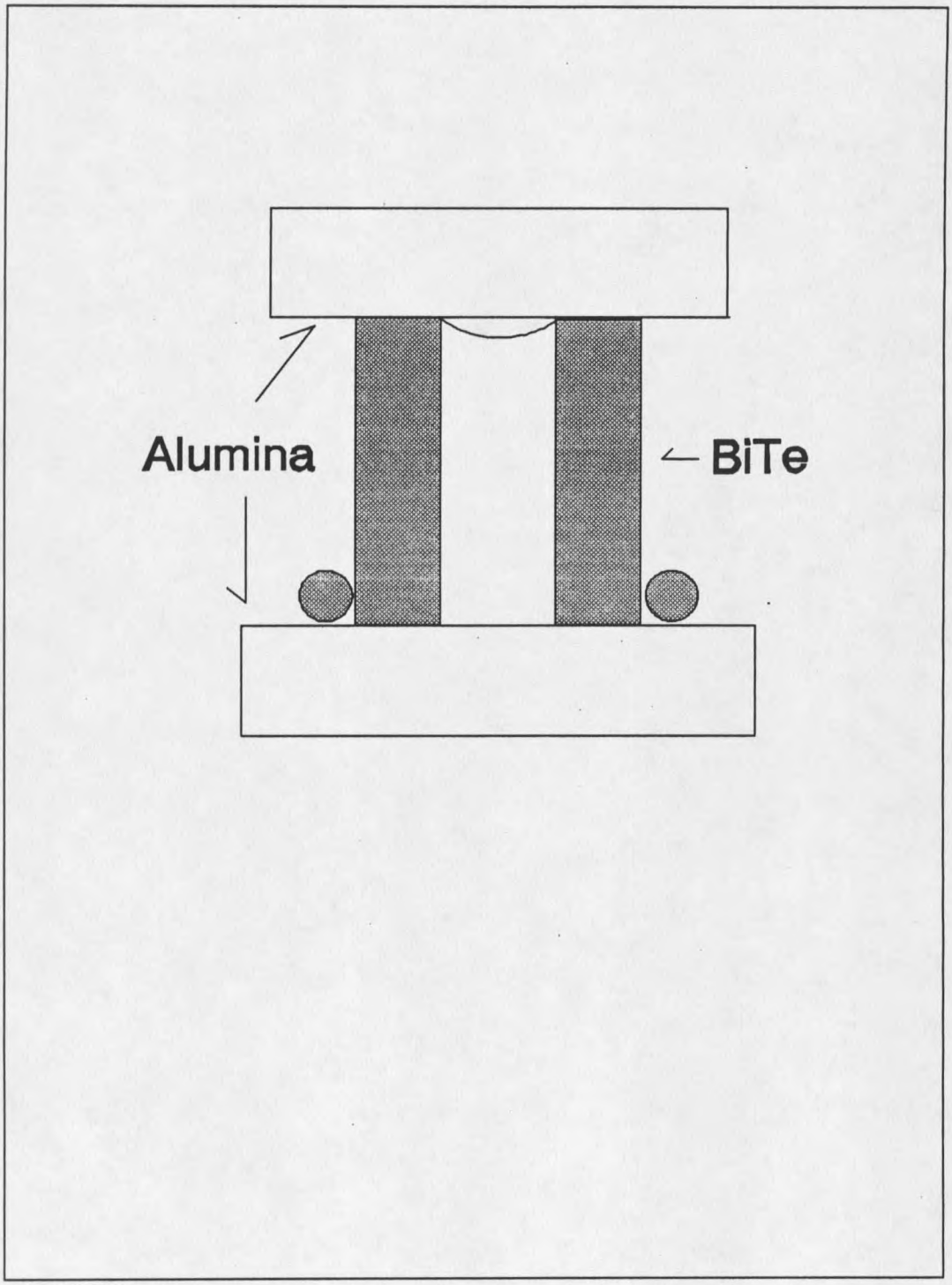

Thermoelectric Device

Figure 3

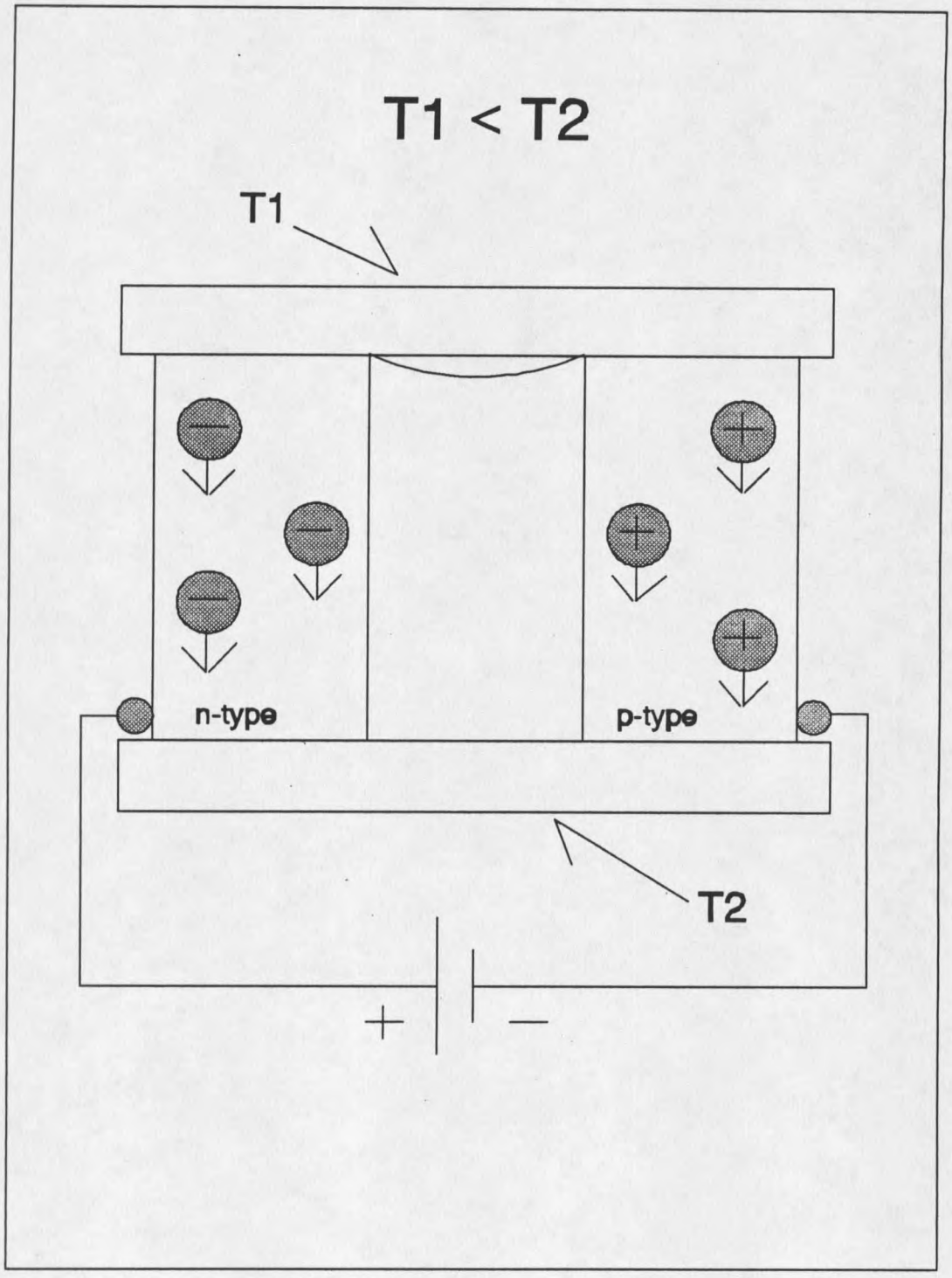

Peltier Effect

Figure 4

Thermocouple Based Mean Temperature Monitoring System

The temperature of the copper slug is continuously monitored by use of a thermocouple attached to its top as shown in Figure 5.

The thermocouple consists of two wires, a chromel-alumel combination, which are soldered together at both ends with a break in one of the wires where terminals of a voltmeter are attached on either side of the break. One soldered end is attached to the copper slug while the other is immersed in an insulated ice bath held at 0°C. Much like the Melcors, the thermocouple makes use of the Seebeck effect.[3] Since the two ends are held at different temperatures an emf is established in the conductors. The value of the thermocouple voltage is then converted through use of a conversion table into a temperature.

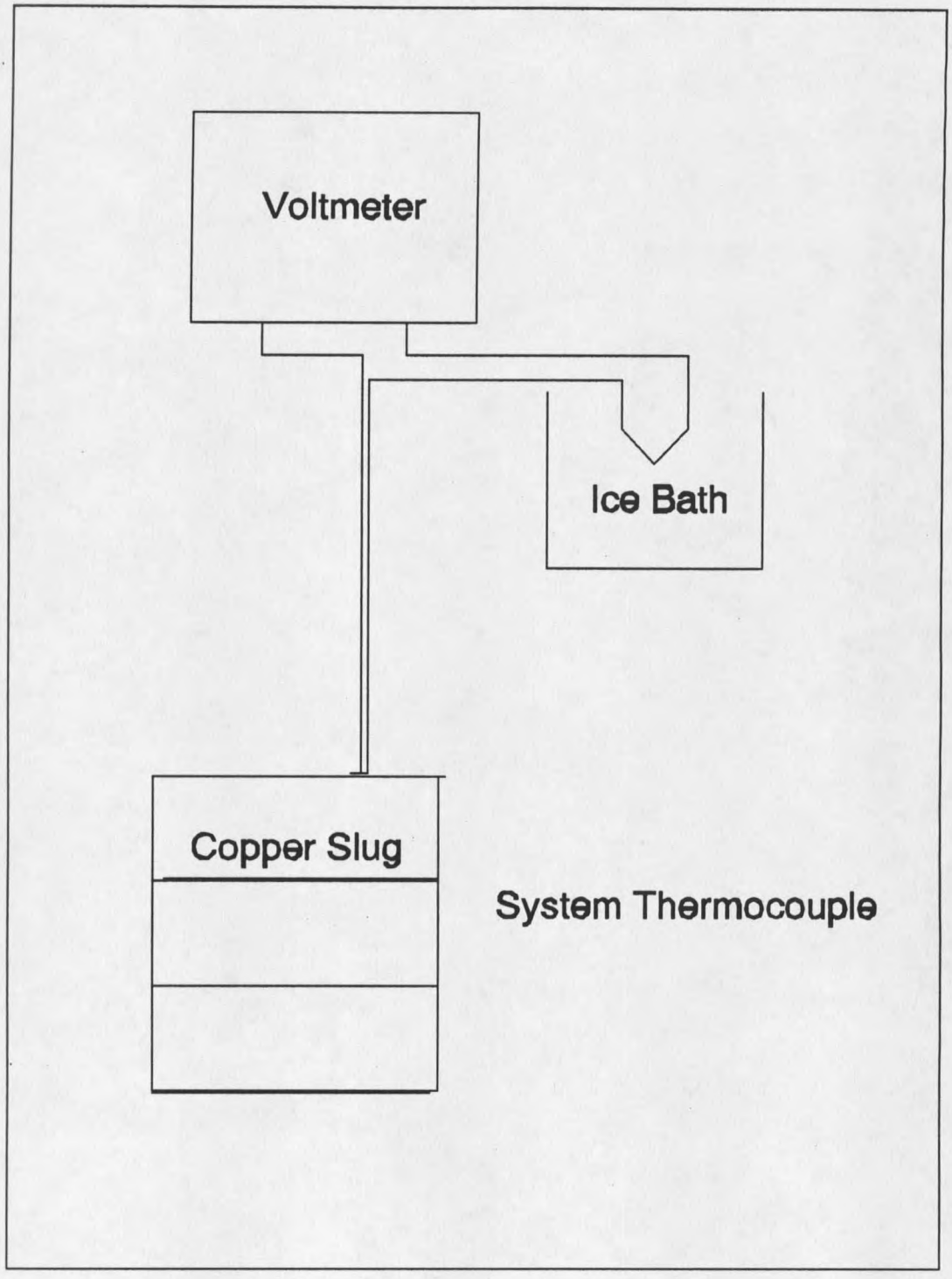

System Thermocouple

Figure 5

Lock-In Amplifier

The lock-in amplifier is the heart of the signal receiving system. It amplifies and measures the receiver signal, and compares the phases of the driver voltage and receiver signal, as shown in Figure 6.

The input reference signal is taken directly from the function generator and provided to the reference circuits. The reference circuits then deliver two output signals, the first with phase φ_2, the second with phase $\varphi_2+90°$, to the in-phase and quadrature mixers respectively. The two mixers are also fed the input signal of phase φ_1.

The in-phase mixer multiplies the input signal by the reference signal, namely

$S_o\cos(\omega t+\phi_1) \times R_o\cos(\omega t+\phi_2) = (1/2)S_oR_o[\cos(2\omega t+\phi_1+\phi_2) + \cos(\phi_1-\phi_2)]$. The low-pass filter located between the in-phase mixer and output filters out the $\cos(2\omega t+\phi_1+\phi_2)$ signal thus yielding $(1/2)S_oR_o\cos(\phi_1-\phi_2)$ as the output. Likewise the action of the quadrature mixer is,

$$S_o\cos(\omega t+\phi_1)R_o\cos(\omega t+\phi_2+90°) = (S_oR_o/2)[\cos(2\omega t+\phi_1+\phi_2+90°) + \cos(\phi_1-\phi_2-90°)]$$

and its low-pass filter eliminates the $\cos(2\omega t+\phi_1+\phi_2+90°)$ signal, yielding $(1/2)S_oR_o\cos(\phi_1-\phi_2-90°) = (1/2)S_oR_o\sin(\phi_1-\phi_2)$.

When $(\varphi_1-\varphi_2)=0°$ the in-phase output is maximum while the quadrature output is zeroed, hence the input and reference signals are in phase. When $(\varphi_1-\varphi_2)=90°$, the in-phase output

is zeroed while the quadrature output is maximum, hence the input and reference signals are in quadrature or 90° out of phase.

In the case when $0° < (\varphi_1 - \varphi_2) < 90°$, the responces of both the in-phase and quadrature outputs will be non-zero.

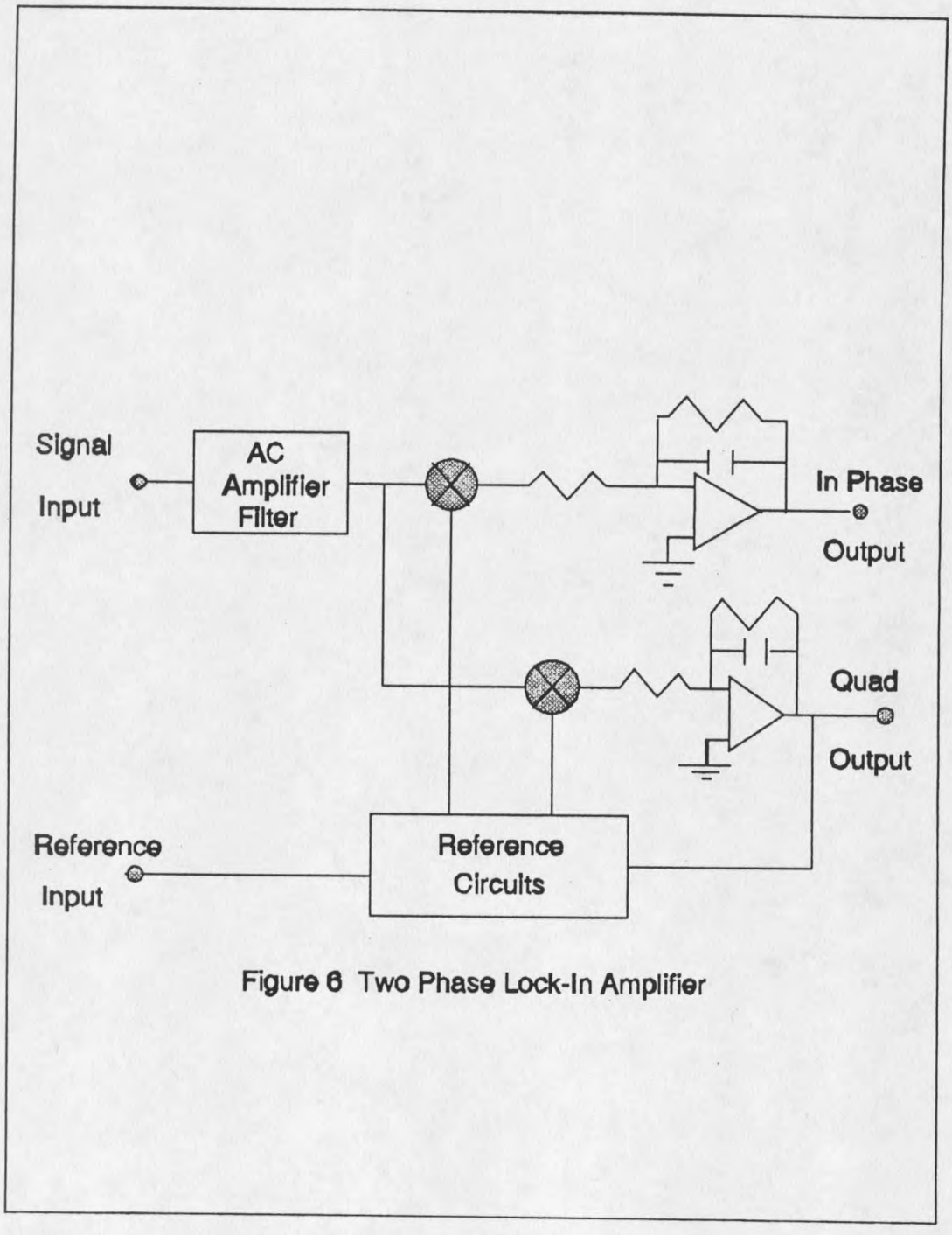

Figure 6 Two Phase Lock-In Amplifier

Two Phase Lock-In Amplifier

Figure 6

CHAPTER 3

EXPERIMENTAL PROCEDURE

The experimental procedure consisted of three areas, the first being system calibration, followed by the dc thermal measurements, and finally ac thermal measurements.

The system calibration included three areas, the Seebeck response of the Melcors, the electrical resistance of the coaxial cables connecting the driver and receiver Melcors to the switch box, and finally the phase calibration of the lock-in amplifier.

The dc thermal measurements consisted of the Melcors being in place on the copper slug and dc voltage signals applied to the driver Melcors and receiving the resulting dc receiver Melcor signals.

The ac thermal measurements were identical to the dc thermal measurements except that ac voltage signals are applied to the driver Melcors and the resulting ac reciever signals are gathered.

System Calibration

Seebeck Response

The thermocouple calibration consisted of two steps. The first involved placing the Melcor device in a known thermal gradient where its voltage response was measured.
This process yielded the Seebeck response for the thermoelectric element. Each Melcor was sandwiched between

two sections of aluminum channel. One section had a power resistor attached to its inside face, and each section had a hole bored vertically halfway down its length in order for thermometers to be placed to monitor the temperature gradient across the Melcor as shown in Figure 7. A dc voltage source was used to energize the power resistor. A voltmeter then monitored the resulting Seebeck voltage as a function of temperature difference between the two alumina faces of the Melcor. Two Melcors were tested separately, and their plots of Seebeck voltage vs. temperature difference are shown in Figures 8 and 9. The apparent hysteresis depicted in Figures 8 and 9 is due to the fact that the Melcors respond faster than the thermometers, shown in Figure 7. Because of this faster response a data point on the cooling cycle with a given ΔT coordinate will have a Seebeck voltage coordinate that is lower in magnitude than a data point on the heating cycle with the same ΔT coordinate. Since the curved portions of Figures 8 and 9 were not used in determining their slopes no error was introduced by them.

Figures 8 and 9 depict both the heating and cooling stages of the process. The slopes of the two sets of data were found by using the curve fitting routine in Sigma Plot, 1.557 mV/C° and 1.593 mV/C° in Figure 8, and 1.610 mV/C° and 1.589 mV/C° in Figure 9. The average of all four slopes is 1.587 mV/C°, which when inverted yields 0.630C°/mV, the

conversion factor necessary to determine the temperature at the receiver Melcor interface from the receiver voltage signal.

Electrical Resistance

The HP3325B function generator supplied 0.5 V_{peak} ac voltage signal to the driver Melcors, each driver channel in turn possessed an inherent resistance which was the equivalent series resistance of the interior and exterior resistance of the coax cables and the resistance of each driver Melcor.

For channel I:

R_{DI} = 2.259Ω ± 0.002Ω, Melcor resistance = 0.547Ω,

For channel II:

R_{DII} = 1.820Ω ± 0.002Ω, Melcor resistance = 0.558Ω,

For channel III:

R_{DIII} = 1.814Ω ± 0.002Ω, Melcor resistance = 0.555Ω.

These resistance values are used in chapter five in calculating the power delivered to the driver Melcors.

Lock-In Amplifier Calibration

The lock-in amplifier was calibrated by connecting it directly to the signal generator. An ac voltage of 0.5 V_{p-p} with a frequency of 30.0 Hz was delivered to both the Reference and the A-Input of the lock-in. This yielded a strong In-Phase signal of 0.175 V_{rms} and a slight quadrature signal of 0.008 V_{rms}.

As the signal strength to the lock-in remained constant and the frequency was decreased finally to 0.5 Hz, the In-Phase voltage remained fairly constant while the quadrature signal steadily increased, finally reaching 0.050 V_{rms}.

Compensation for this phase error was accomplished at each frequency by depressing the 0° Reference button of the Lock-In and rotating the Phase dial clockwise until the quadrature signal equaled zero.[15] Since the In-Phase and Quadrature meters are analog, these meter voltages were digitized and displayed by an HP 34401A multimeter coupled to the meters by the I-Out and Q-Out ports of the Lock-In. The results of these measurements are found in Table 1.
The next step consisted of the dc thermal conductivity measurements. The Melcor devices were arranged with no sample in channel I, with a lead metal sample on channel II, and a triglycine fluoberyllate (TGFB) crystal sample on channel III as the drivers are given a dc voltage signal to which the receivers must respond.

DC Thermal Measurements

The dimensions of the lead sample are 0.67 mm thick x 3.24 mm x 1.33 mm, while those of the TGFB sample are 0.48 mm thick x 2.20 mm x 2.86 mm. Figure 10 shows the voltage responses of the receiver Melcors when dc voltages over the range -500 mV < V_{driver} < 500 mV are applied to the driver

Melcors with no samples present. Figure 11 shows the voltage responses of the receiver Melcors when dc voltages over the range $-500mV < V_{driver} < 500mV$ are applied to the driver Melcors when the lead sample is on channel II and TGFB on channel III. Again using the curve fitting routine of Sigma Plot the slopes of the data from the three channels were found to be 0.0797, 0.0900, and 0.0659. This information is critical for the dc limit of heat flow through the system.

AC Thermal Measurements

The main part of the experiment was conducted at room temperature, using sinusoidal driving voltages at different frequencies to determine thermal diffusivity, thermal conductivity, and specific heat.

The frequency was stepped logarithmically beginning at 0.5 Hz and ending at 30 Hz. At each frequency, the driving voltage was applied to each channel in turn, and the sensor response was read from the lock-in amplifier's In-Phase and Quadrature voltage dials. The process was repeated as the system temperature was varied $+25°C < T_{sys} < +80°C$.

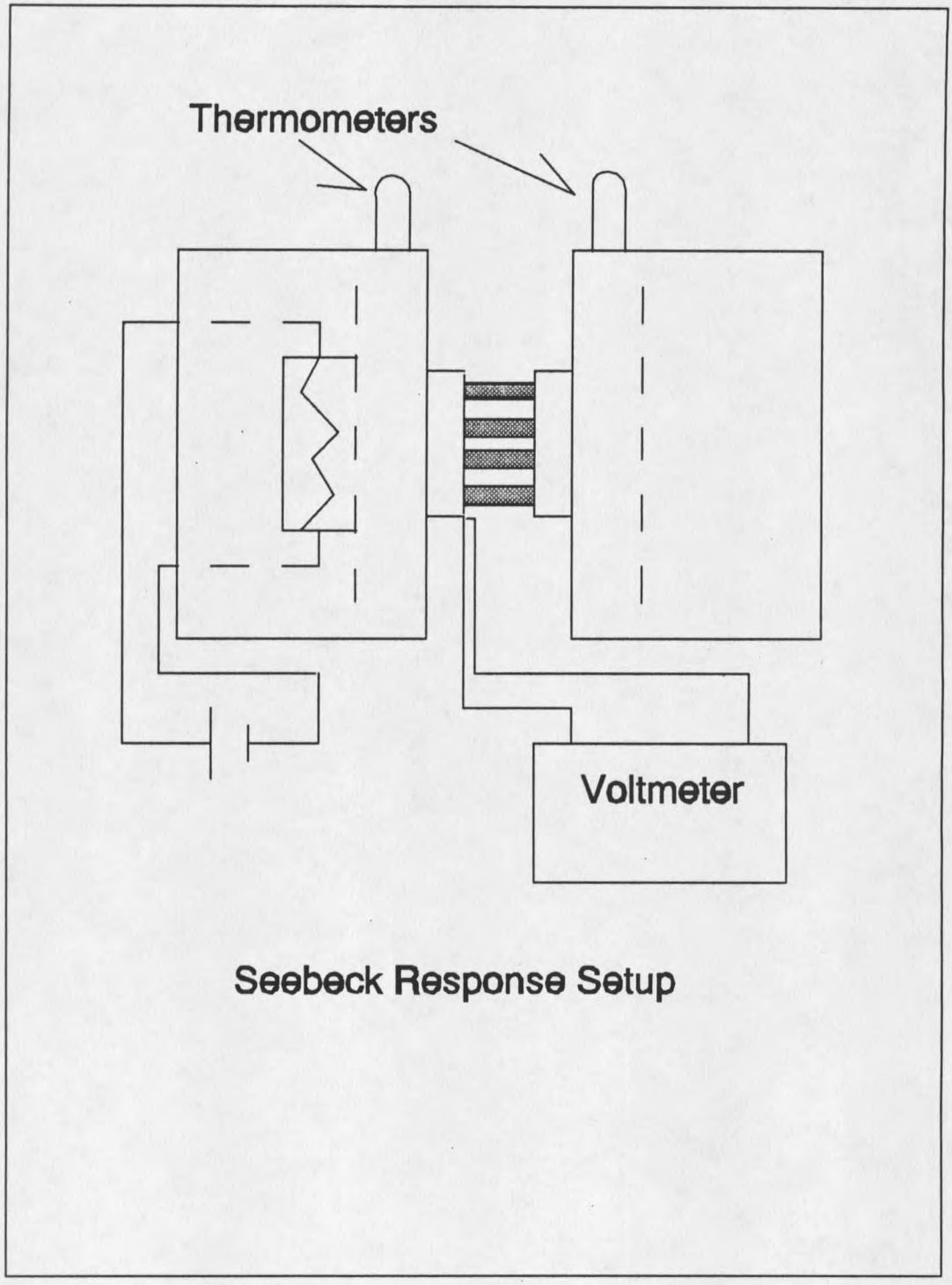

Seebeck Response Setup

Figure 7

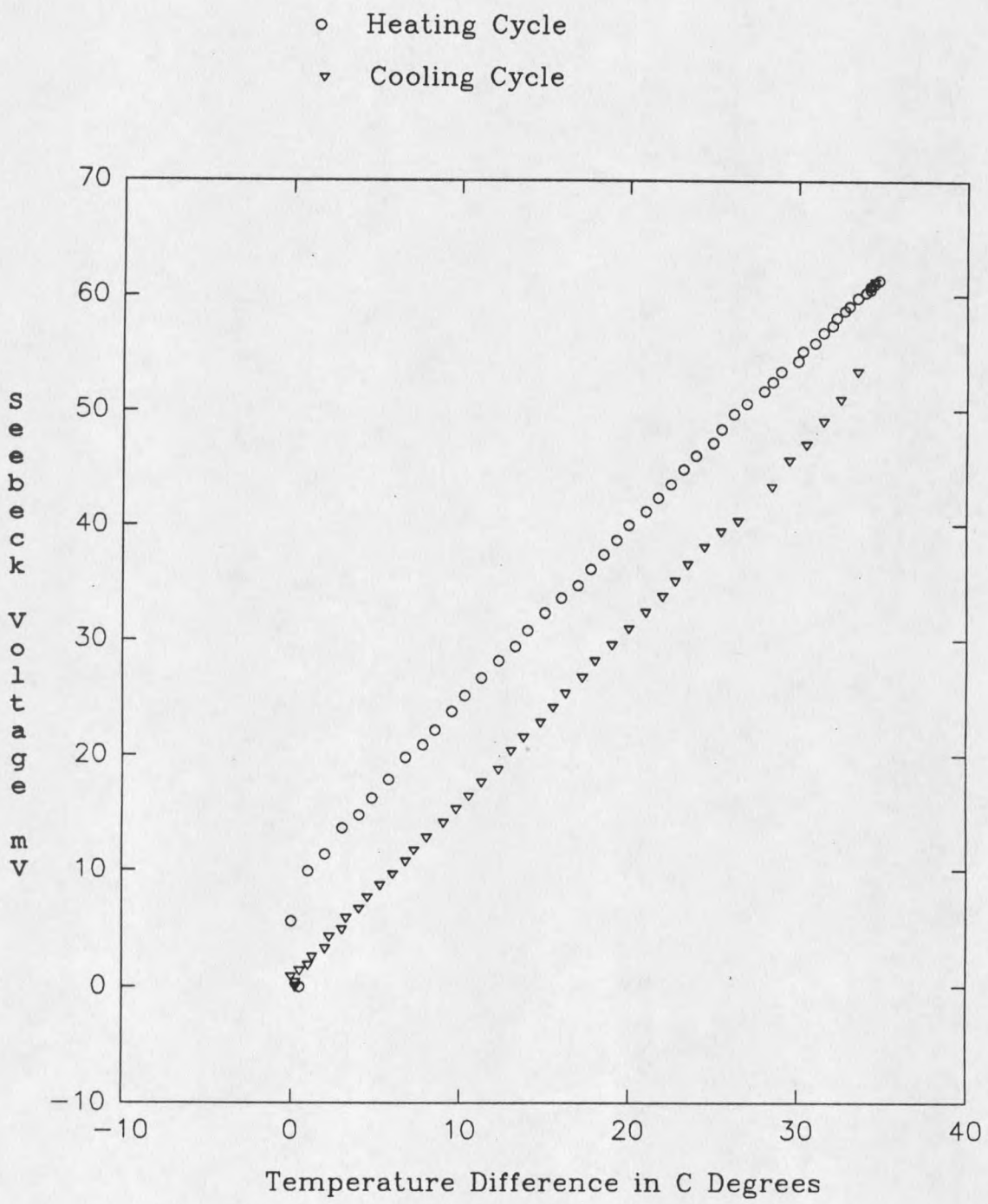

Seebeck Calibration

Figure 8

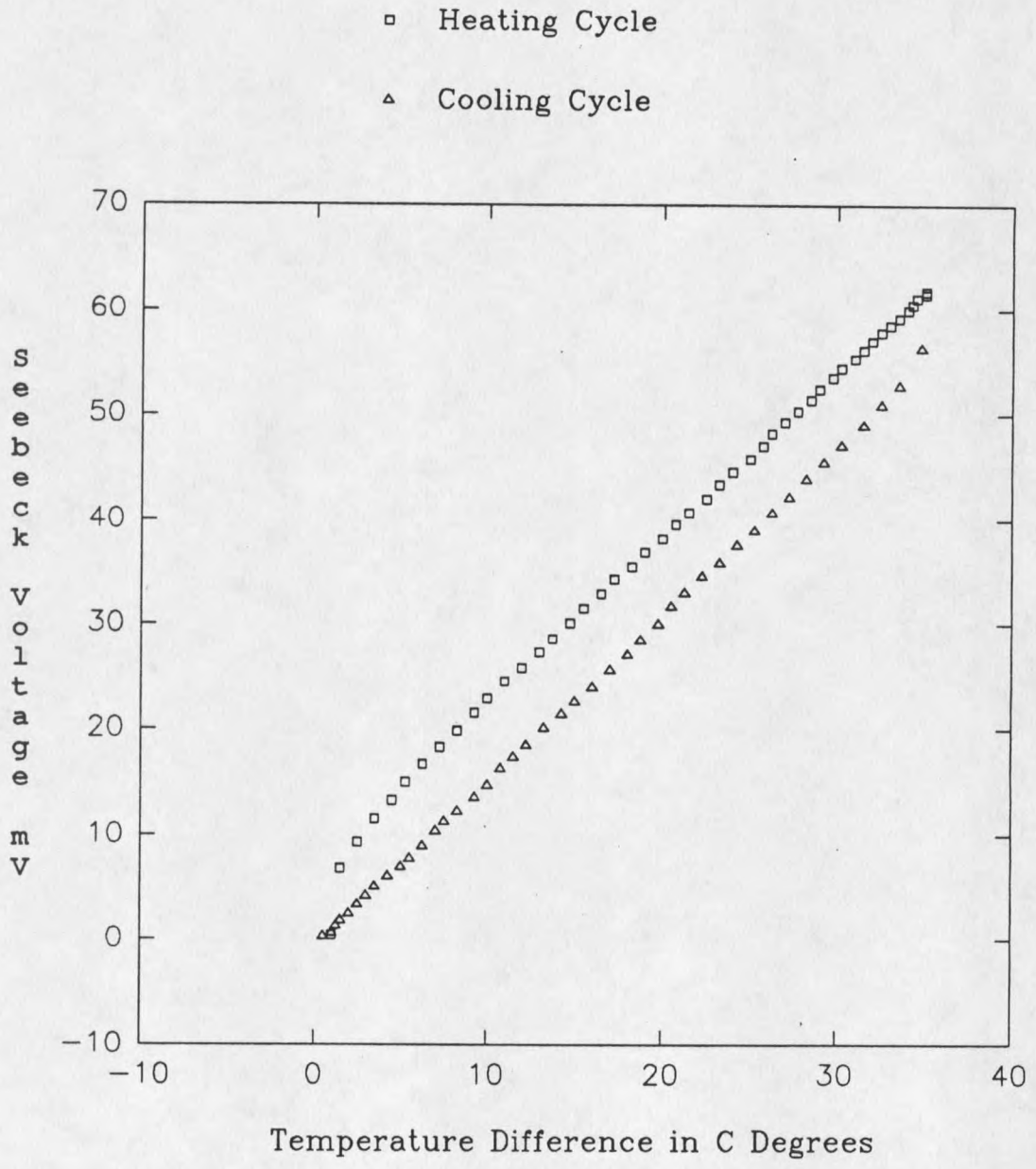

Seebeck Calibration

Figure 9

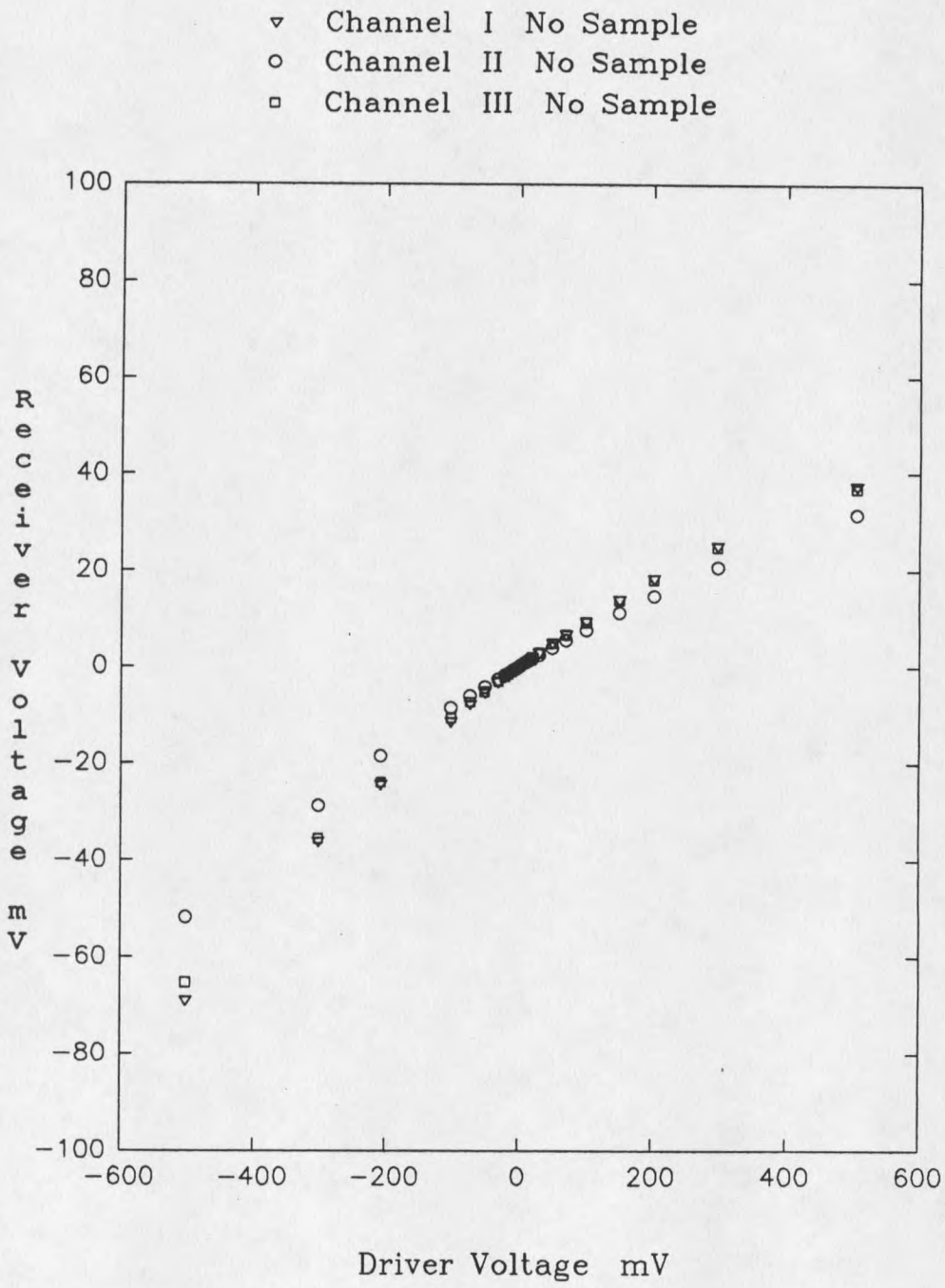

DC Calibration Without Samples

Figure 10

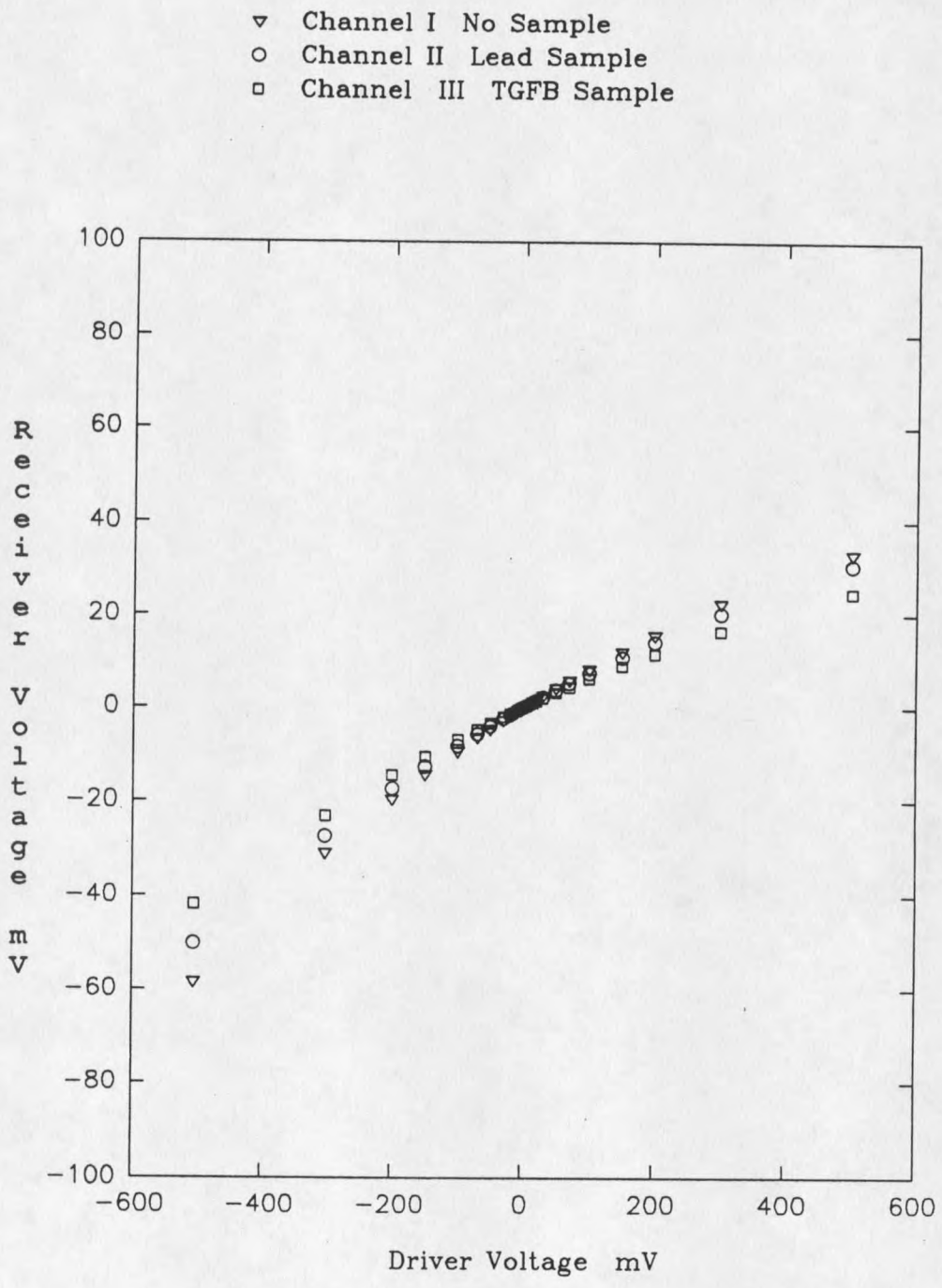

DC Calibration With Samples

Figure 11

Frequency	Phase Dial Setting
30.0 Hz	+ 3.2°
20.0 Hz	+ 3.3°
15.0 Hz	+ 3.4°
10.0 Hz	+ 3.6°
7.0 Hz	+ 3.8°
5.0 Hz	+ 4.2°
3.0 Hz	+ 4.9°
2.0 Hz	+ 5.9°
1.5 Hz	+ 6.6°
1.0 Hz	+ 7.9°
0.7 Hz	+ 10.0°
0.5 Hz	+ 12.4°

Lock-in Amplifier Phase Zeroing

Table 1

CHAPTER 4

DEVELOPMENT OF THE SYSTEM

The process of developing this system into a working prototype followed an interesting learning curve. There were five major design problems which were encountered and solved, namely impedance mismatches, cross talk between channels, EMI shielding, ground loops, and eliminating heat convection in the sample chamber.

The first problem, impedance mismatch, existed between the function generator, which had an output impedance of 1 Megohm, and the thermoelectric elements, each possessing a resistance on the order of 1 ohm. This problem was solved by using a unity gain amplifier, constructed in-house, to match the two impedances.[13]

The next three problems, cross talk between channels, ground loops and EMI shielding, were interrelated.

The initial wiring of the probe used unshielded single conductor wire which connected the electrodes of the copper slug to the BNC connectors at the top of the probe. Inevitably the wires would tangle inside the stainless steel tube producing one source of cross talk. The fact that not all the electrodes on top of the copper slug were isolated also produced a related problem of ground loops and hence a second contributor to the cross talk problem.

This became evident when the first trial measurements were run and all three channels yielded the same voltage values, namely the strongest signal would be dominating. The use of coaxial cables was the first step to eliminate cross talk between the signal channels.

The ground loops initiating at the electrodes of the copper slug were easily eliminated by using insulated wiring posts to make the "return wire" connection of each thermoelectric element isolated from all the other thermoelectric element connections. The "positive" wires of each thermoelectric element were already connected to isolated wiring posts. The cross talk-ground loop problem still remained, but was narrowed down to two areas, the top of the probe and at the switch box. Once it was discovered that each channel's signal "return" path had a common electrical connection through the aluminum flange of the top of the probe and through the aluminum top plate of the switch box it was clear how the signals were mixing.

I was then unaware of the existence of floating BNC connectors, so my first solution to this problem was to make the top flange of the probe and the top plate of the switch box from Plexiglas material. The next set of trial data showed distinctive signals on all three channels, but electrical noise was also present.

The noise sources were determined to be the ambient environment of the laboratory and the bipolar power supply,

which energizes the unity gain amplifier.

The discovery of the ambient laboratory noise motivated the search for some sort of insulated BNC connector which would allow the top flange of the probe and the top plate of the switch box to be made from aluminum and hence electrically connected to a common electrical ground point. This was likewise the solution for the bipolar power supply; the Plexiglas shields were replaced with aluminum plates and electrically grounded at the same point.

To insure proper EMI shielding, all conductive surfaces are connected electrically to the ac line ground of the bipolar power supply.

After some initial data were gathered and analyzed, the next problem was encountered; the data did not fit theory as well as expected.

We decided to improve the apparatus design in hopes of obtaining better results.

The first improvement was to remachine the surfaces upon which the Melcor elements were bonded. By milling radial grooves the same distance away from the cylindrical axis of the copper slug on both the top cylinders and the moveable stages, Figures 12 and 13, the face-to-face alignment of all three Melcor pairs was improved.[13,16]

It was next decided to eliminate the possibility of convection heat transfer in the sample chamber. The first step in achieving this was to use small O-rings and washers

with the screws which attached the bottom flange and the copper can to the copper slug.

The second step was to apply RTV Silicone sealer at the junction of the top flange and the stainless steel tube, where the coaxial cables were terminating. The first step worked but the second step failed repeatedly. The solution to sealing that junction was to use a Teflon feed-through plug, shown in Figure 14.[16] One final vacuum problem remained, which was the O-ring at the copper can - bottom flange junction. The solution was simply to machine a wider O-ring grove in the bottom flange so an O-ring of greater cross-sectional diameter could be used.[16]

With the vacuum problems resolved and adjustments made to the Band-Pass setting of the lock-in amplifier, data gathering was resumed.

An important improvement in gathering the data was made. Initially the In-Phase and Quadrature voltages were read directly from the analog meters. This inefficient and inaccurate method of gathering data was modernized by computer interfacing together the lock-in amplifier, function generator, plotter, and a personal computer (PC) as shown in Figure 15. This partial automization of the system resulted in more accurate in-phase and quadrature voltage values and a significant reduction in data collecting time.[17]

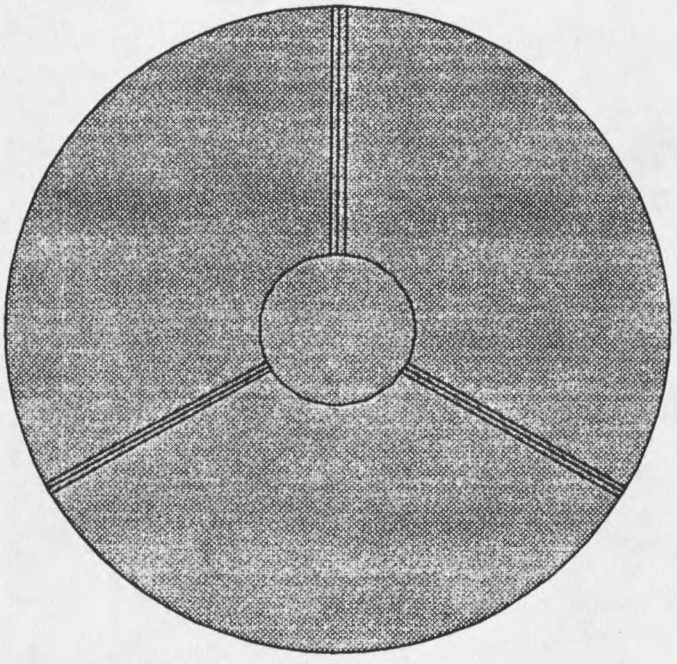

Remachined Top Cylinder

Figure 12

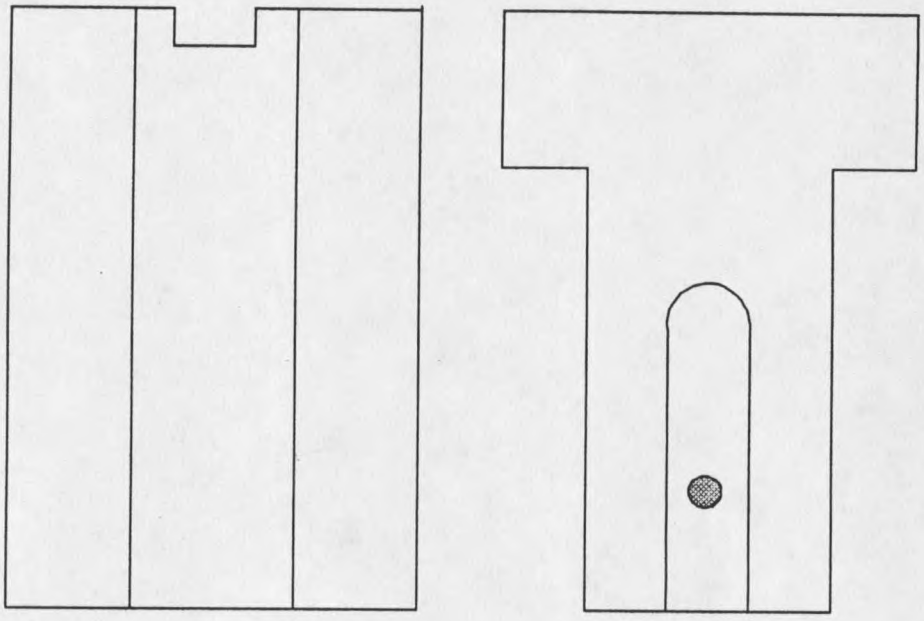

Remachined Moveable Stage

Figure 13

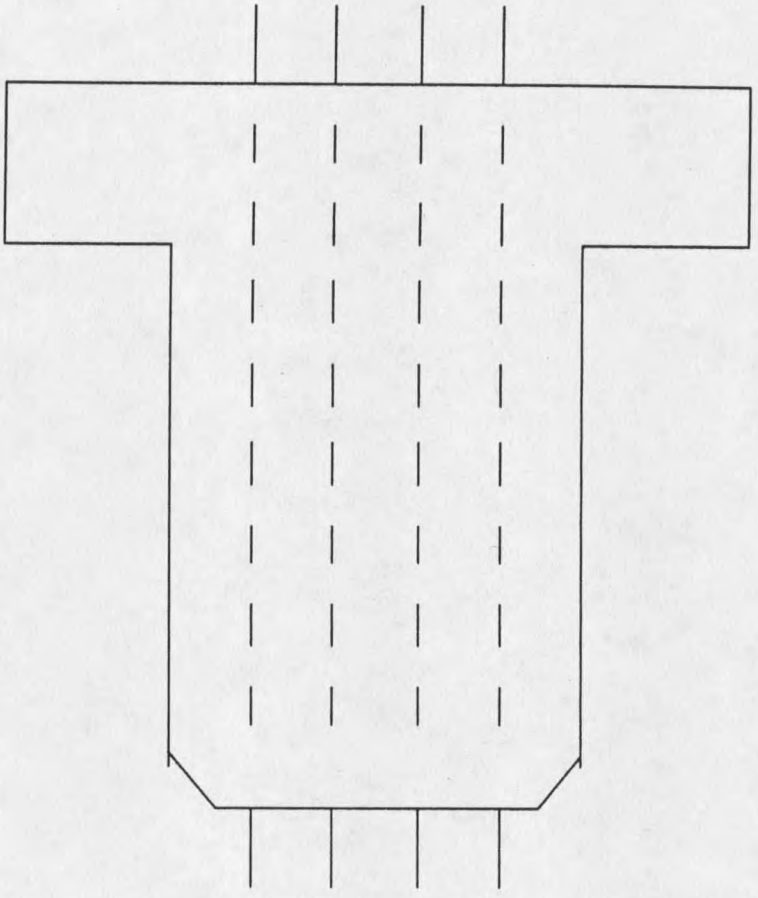

Teflon Feedthrough

Figure 14

The components that were connected via GPIB (General Purpose Interface Bus) cables were the function generator, the plotter, and the PC. Since the lock-in amplifier does not have GPIB capability, the in-phase and quadrature meter voltage signals were linked to the plotter via coaxial cables, and the plotter then functioned as an analog-to-digital conversion board. A computer program written in Pascal was used to send instructions to the function generator and the plotter for changing frequency, gathering and sending data.

Once the partial automation of the system was established, the quest for good data resumed. After several runs, it was clear that the high frequency data points showed the expected steady diminishing in amplitude and increasing in phase angle with frequency. However, some low frequency data points displayed an amplitude too great or a grossly incorrect phase with respect to their neighboring data points. These errors were seen in the data of all three channels. Since it seemed unlikely that all three pairs of Melcor elements would be failing, a problem with the signal generating or signal receiving components seemed likely. After thorough trouble shooting of the entire system it was found that an intermittent failure of the lock-in amplifier was the cause of the spurious data. This problem was solved by borrowing a lock-in amplifier of identical type from the adjoining laboratory, which when integrated into the system

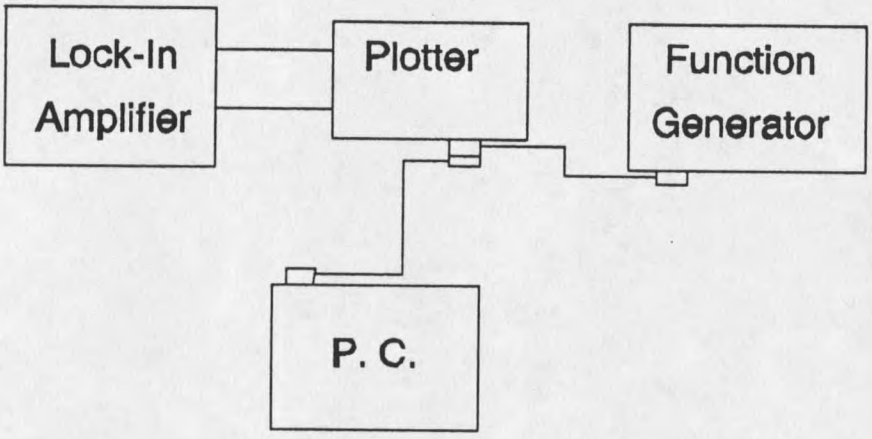

Computer Interfaced Components

Figure 15

performed consistently well.

The first set of good consistent data gathered at room temperature is shown in Tables 2, 3, and 4. The data is ploted in Figures 16, 17, and 18.

The next step in the development of the apparatus was to make measurements over a temperature range, specifically to make measurements on TGFB (triglycine fluoberyllate) between 25° C and 80° C, to search for thermal anomalies near the ferroelectric transition temperature at 70° C.[2]

The first attempts at traversing this temperature range were unsuccessful because the vacuum jacket of the dewar had been breached, so the heater could not raise the temperature sufficiently. The solution was to pump on the vacuum jacket with a roughing pump to achieve a pressure of 10^{-2} torr, followed by a diffusion pump to bring the pressure of the vacuum jacket to $6x10^{-6}$ torr.

The next attempt at gathering data on TGFB over the temperature range +25°C to +80°C uncovered yet another problem. At +74°C and at +76°C a fluctuation in the voltage of the thermocouple monitoring the temperature of the copper slug was observed. This fluctuation corresponded with the turning on of the roughing pump used to evacuate the sample chamber before each data run. This observation led to the discovery of another ground loop. The loop consisted of the thermocouple junction in physical contact with the copper slug and the system ground wire, which was also in physical

Frequency	Temperature	Phase Angle
0.5 Hz	0.756 ± 0.005 K	-101.9 ± 0.8°
0.7 Hz	0.530 ± 0.005 K	-109.3 ± 1.8°
1.0 Hz	0.363 ± 0.004 K	-116.8 ± 0.5°
1.5 Hz	0.227 ± 0.002 K	-129.4 ± 0.4°
2.0 Hz	0.156 ± 0.001 K	-140.0 ± 0.2°
3.0 Hz	0.085 ± 0.001 K	-156.9 ± 0.5°
5.0 Hz	0.036 ± 0.0002 K	-179.4 ± 0.7°
7.0 Hz	0.0188 ± 0.0001 K	+164.0 ± 0.7°
10.0 Hz	0.0087 ± 0.0006 K	+144.4 ± 7.9°
15.0 Hz	0.0033 ± 0.0003 K	+122.0 ± 11.8°

Measured Temperature for No Sample

Table 2

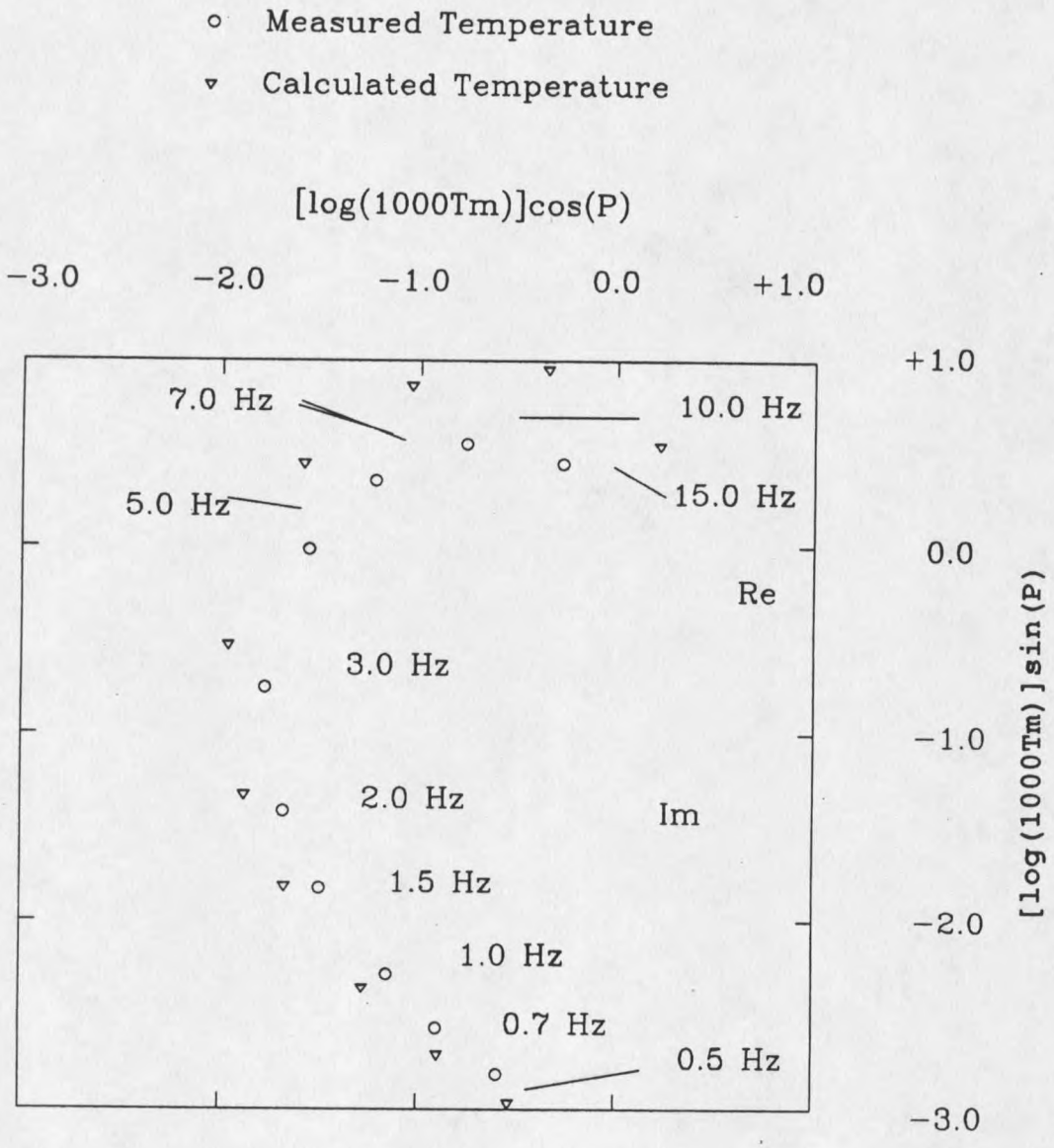

Logarithmic Polar Plot of Complex Temperatures at Sensor

No Sample

Figure 16

Frequency	Temperature	Phase Angle
0.5 Hz	0.6470 K	-119.4°
0.7 Hz	0.4246 K	-130.9°
1.0 Hz	0.2604 K	-143.1°
1.5 Hz	0.1411 K	-160.0°
2.0 Hz	0.0870 K	-171.6°
3.0 Hz	0.0413 K	+168.3°
5.0 Hz	0.0143 K	+141.3°
7.0 Hz	0.0065 K	+119.5°
10.0 Hz	0.0020 K	+ 81.2°
15.0 Hz	0.0007 K	- 10.5°

Measured Temperature for Lead Sample

Table 3

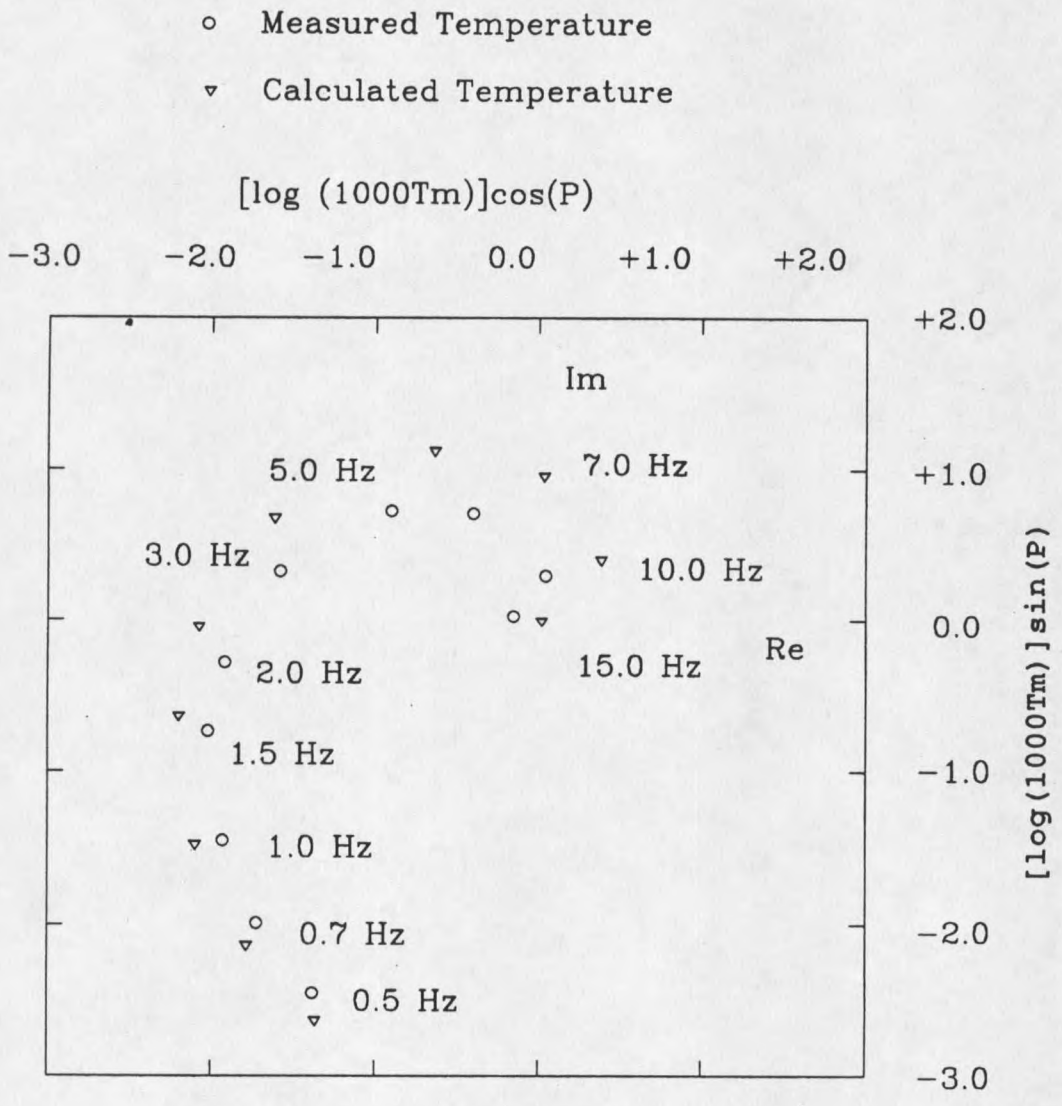

Logarithmic Polar Plot of Complex Temperatures at Sensor Lead Sample

Figure 17

Frequency	Temperature	Phase Angle
0.5 Hz	0.09770 K	+157.3°
0.7 Hz	0.05229 K	+142.6°
1.0 Hz	0.02331 K	+123.8°
1.5 Hz	0.00847 K	+ 97.1°
2.0 Hz	0.00380 K	+ 74.4°
3.0 Hz	0.00106 K	+ 36.7°

Measured Temperature for TGFB Sample

Table 4

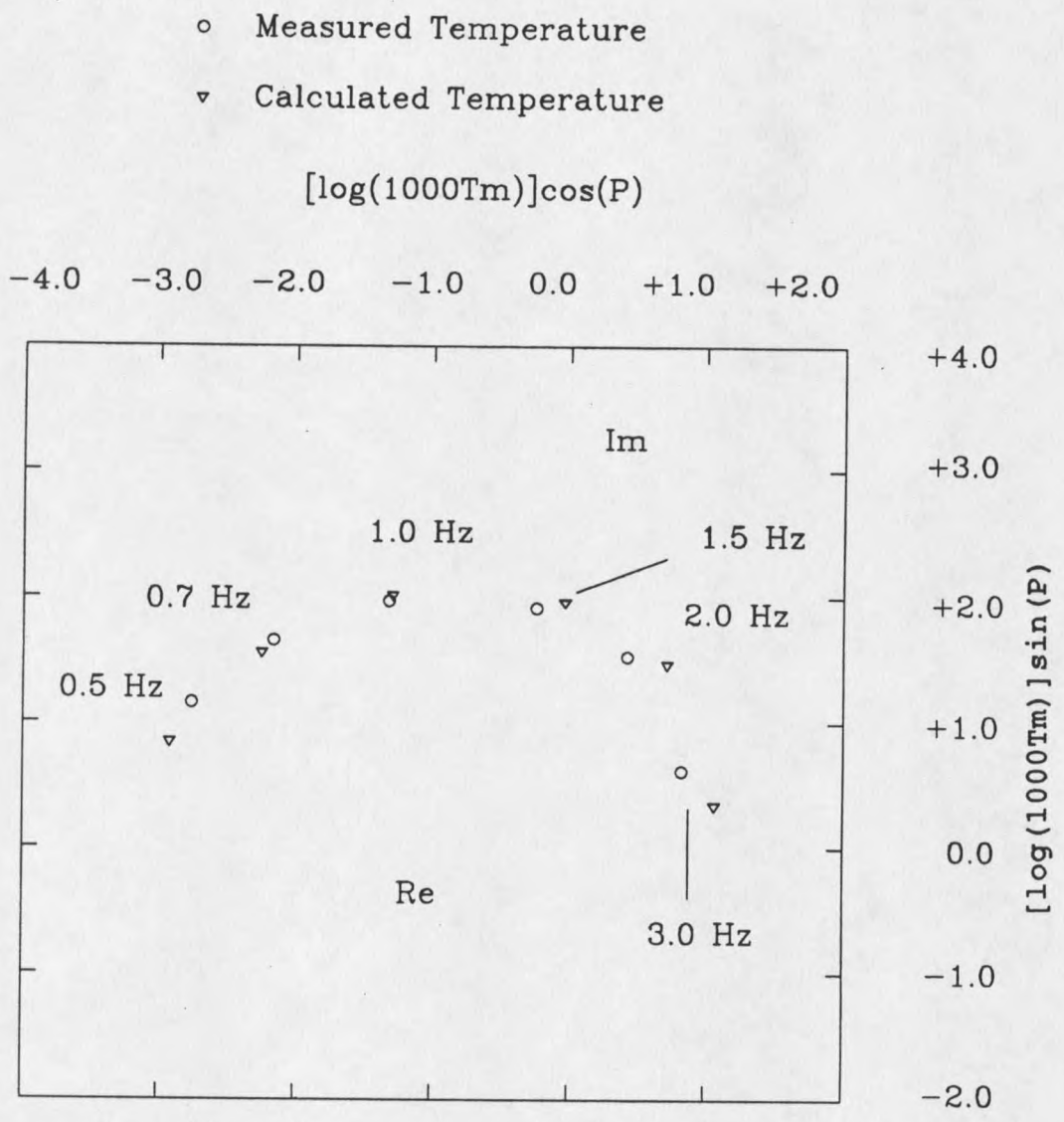

Logarithmic Polar Plot of Complex Temperatures at Sensor TGFB Sample

Figure 18

△ System Temperature = +70 C

▲ System Temperature = +75 C

○ System Temperature = +80 C

▼ System Temperature = +75 C

▽ System Temperature = +70 C

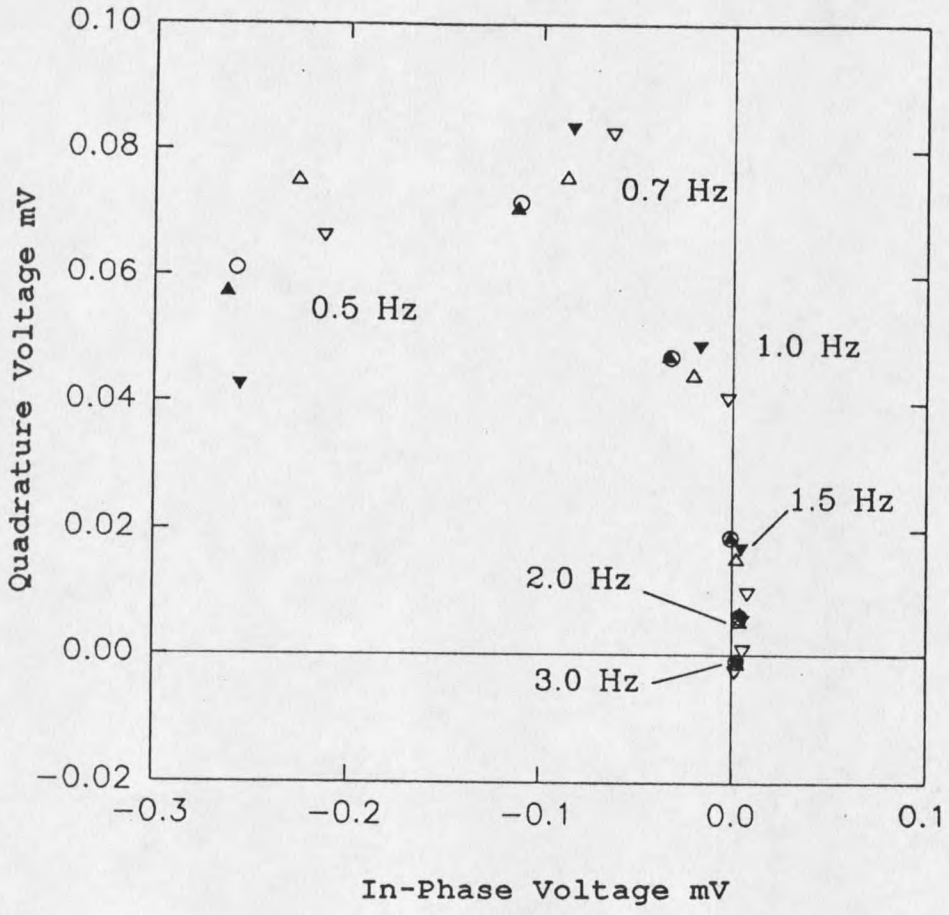

Response of TGFB over Frequency Range

0.5 Hz to 3.0 Hz

Figure 19

contact with the copper slug.

The electrical resistance between the thermocouple wire at the voltmeter and the copper slug was found to be 6.0 Ω.

Hence any variation in electrical ground voltage was easily detected through the thermocouple wire. The voltage variation was of the order of 200 μV which corresponds to approximately a 5 °C temperature variation.

The solution was to electrically isolate the thermocouple wire from the copper slug yet maintain its thermal contact with the copper slug. This was achieved by wrapping the thermocouple junction with a layer of Teflon tape and securing the junction to the copper slug with a nylon washer and nylon screw. The thickness of the Teflon tape layer is 0.075 mm.

The resistance between the thermocouple wire and the copper can was then found to be 36 MΩ. The next attempt at gathering data on TGFB was successful over the temperature range of +25°C to +80°C, then back down to +70°C, as shown in Figure 19.

CHAPTER 5

THEORY

The flow of heat in the solid samples is modeled in two ways, namely a steady state or dc model and an ac heat flow model. First, the dc model will be described along with the calculation of the thermal conductivities k_{Pb} and k_{TGFB} of the Pb and TGFB samples. This will be followed by the description of the ac heat flow model and the calculation of the heat flux input J_{IN} at the driver Melcor, beginning from T_m, the measured temperature at the receiver Melcor.

DC Heat Flow Model

The dc heat flow model is a thermal circuit which is analogous to an electrical circuit. Here heating/cooling power is analogous to electrical current, temperature is analogous to voltage, and thermal resistance analogous to electrical resistance. The first case is that of no sample between the driver and receiver Melcors. The circuit is shown in Figure 20. The resistor symbols, R_{Alu} and R_{BT} are the thermal resistances of the alumina and bismuth telluride layers respectively. The independent power source P_o represents the thermoelectric power delivered to or removed from the bismuth telluride - alumina interface of the driver Melcor. The voltmeter which accepts signals from the receiver Melcor is represented by V.

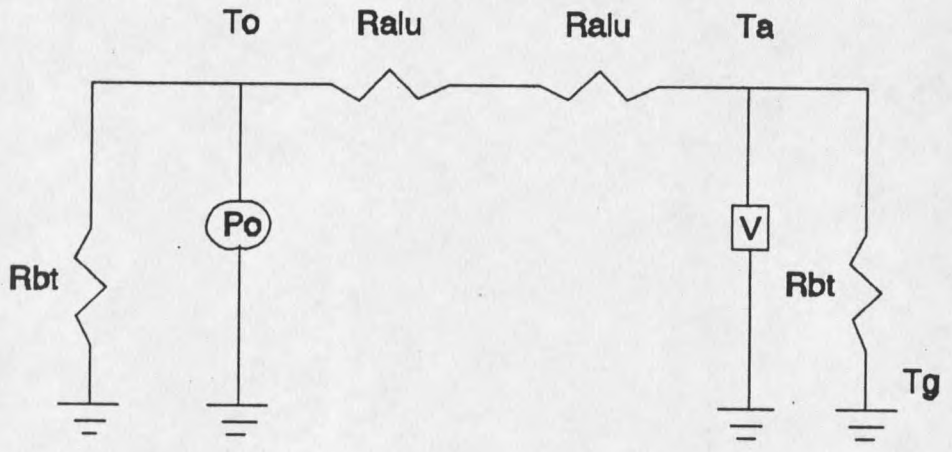

DC Thermal Circuit No Sample

Figure 20

The input heating power P_o has the form, $|P_o| = (0.500)I + (0.281)I^2$ for the heating cycle, $|P_o| = (0.500)I - (0.281)I^2$ for the cooling cycle, where P and I are in watts and amperes respectively. The voltage value from the receiver Melcor is multiplied by the factor 0.63 K/mV, derived as described in Chapter 3, to yield a temperature value. The ground symbols represent thermal ground which is the copper slug.

The data gathered in this part of the experiment enabled the calculation of the thermal resistance of the Bi_2Te_3 pillars of the Melcors. These thermal resistance values were determined by dc circuit analysis methods. Applying Kirchhoff's voltage law to both the right and left loops of the thermal circuit yields the expressions:

$$T_0 = P_0[(R_{BT}R)/(R + R_{BT})] \quad (5\text{-}1)$$

$$T_1 = P_1R_{BT} \quad (5\text{-}2)$$

$T_2 = P_2R$ (5-3) , where $R = 2R_{Alu} + R_{BT}$, along with P_1 and P_2 which are the "thermal currents" of the left and right loops respectively. The "thermal voltages" or temperatures T_0, T_1, and T_2 are all equal, so T_0 and T_2 can be equated yielding:

$$P_2 = P_0R_{BT}/[2(R_{BT} + R_{Alu})] \quad (5\text{-}4) \ .$$

Figure 20 can yield another relation, $P_2 = (T_A - T_G)/R_{BT}$, $(T_A - T_G)$ is the "thermal voltage" across the right R_{BT}, which when equated to (5-4) yields an equation quadratic in R_{BT}.

Using the quadratic formula R_{BT} is found to be:

$R_{BT} = [V + (V^2 + 2P_0VR_{Alu})^{1/2}]/P_0$ where V is the voltmeter voltage which is converted into temperature.

The next step was to insert an "unknown" lead (Pb) sample between the driver and receiver Melcors, as modeled in Figure 21. The data gathered from this configuration of the system allowed the value of the Pb sample's thermal resistance to be calculated. The procedure is the same as that for calculating the thermal resistance of bismuth telluride.

The loop equations of Figure 21 yield:

$$T_0 = P_0[(R_{BT}R)/(R + R_{BT})] \quad (5\text{-}5)$$

$$T_1 = P_1R_{BT} \quad (5\text{-}6)$$

$$T_2 = P_2R \quad (5\text{-}7) \quad \text{where } R = (2R_{Alu} + R_{Pb} + R_{BT}).$$

Once again an equation quadratic in R_{BT} is generated, and solving for R_{Pb} yields:

$$R_{Pb} = [(P_0/P_2) - 2]R_{BT} - 2R_{Alu} \quad (5\text{-}8) .$$

Using the manufacturer's value for R_{Alu},[11] and the above calculated values of R_{BT}, P_0, and P_2, the value of R_{Pb} can be calculated. The next step is to determine k_{Pb}, where thermal resistance is defined, $R_x = (y_2-y_1)/(k_xA)$ where (y_2-y_1) = length of material, k_x = thermal conductivity of the material, and A = cross sectional area of the material. The thermal conductivity of the unknown sample then is:

$$k_x = (y_2-y_1)/(R_xA) \quad (5\text{-}9) .$$

The dimensions of both the lead and TGFB samples are known,

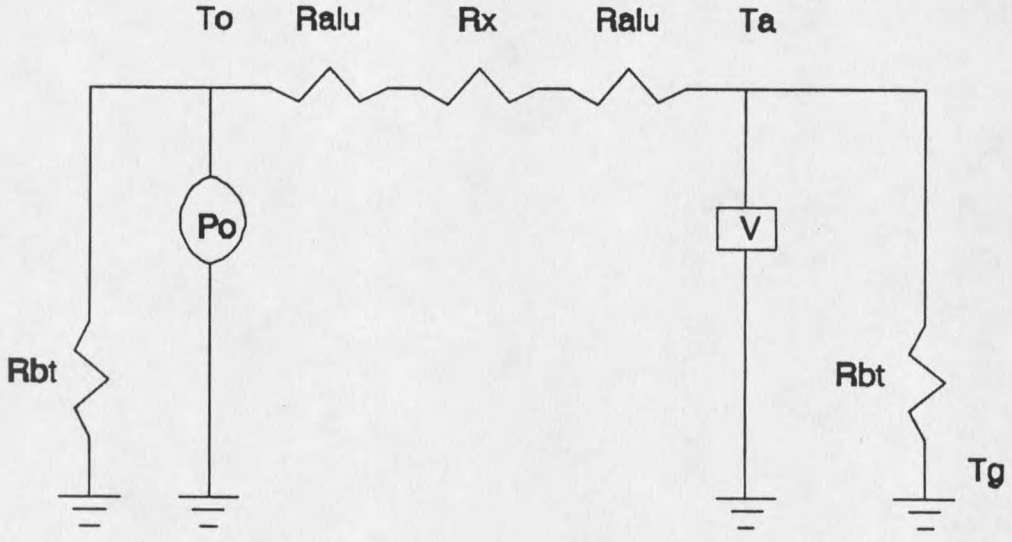

DC Thermal Circuit With Sample

Figure 21

and the effective values of k_{Pb} and k_{TGFB} were found to be k_{Pb} = 2.12 W/m-K and k_{TGFB} = 0.254 W/m-K. The accepted value of thermal conductivity for lead is 34.34 W/m-K.[18] This discrepancy can be explained by an excess amount of thermal grease between the lead sample and the driver and receiver Melcors. Since the calculated value of k_{Pb} is 2.12 W/m-K the corresponding thermal resistance is (m-K/2.12W)(155.5/m) = 73.255 K/W, where 155.5/m is the thickness of the lead sample divided by the area of the lead sample. Likewise, using the accepted value of k_{Pb} in the calculation yields 4.53 K/W. Thus the excess thermal resistance is, 73.25 K/W - 4.53 K/W = 68.72 K/W. The thermal conductivity of the thermal grease is k_G = 0.42 W/m-K [19] from which the thickness of the grease can be calculated. The thermal grease is named Heat Sink Compound 304, Dow-Corning Chemical Co. with a heat capacity per unit volume, C_{grease}= 2.00 x 10^6 J/(m^3K).[19]

$$\Delta x_G = (68.72\ K/W)(0.42 W/m\text{-}K)(4.31 \times 10^{-6} m^2) \quad (5\text{-}10)$$

$$\Delta x_G = 0.124\ mm \quad (5\text{-}11)$$

When this thickness of thermal grease is divided by two the thickness of each layer is x_{layer} = 0.062 mm. So reducing the thickness of the grease layer on each side of the lead sample by a factor of ten would reduce the excess thermal resistance to 0.855 K/W.

For the case of TGFB an accepted value of thermal conductivity couldn't be found so the accepted value for

TGS, k_{TGS} = 0.64 W/m-K was used as a reference which is triglycine sulfate. [20] TGS is also a ferroelectric crystal. Comparison with the value k_{TGFB} = 0.254W/m-K calculated from our data shows that another discrepancy exists. Two factors are possible contributors to this discrepancy, the first being an excess of thermal grease and the second being transverse cracks in the TGFB crystal. Following the development above for lead, the calculation to determine the amount of excess thermal grease on the TGFB crystal is conducted the same way, yielding a layer of thermal grease 0.37 mm thick on each side of the TGFB crystal. This value seems a bit high which raises the probability that transverse cracks are the problem. Such cracks would separate adjacent layers by thin air gaps, interrupting the crystalline structure and the normal heat transfer mechanism.

Finally, in both the case of lead and TGFB, the quality of the interface of each sample with its respective driver and receiver alumina layers needs to be considered. Polishing the mating faces of the lead and and TGFB samples and possibly the alumina faces as well would certainly improve thermal contact. Also, an alternate heat sink compound with a higher thermal conductivity value than the current material, coupled with a consistent method of applying a suitably thin layer would also improve thermal contact.

AC Heat Flow Model[12,21]

In the ac heat flow model we shall make use of temperature waves propagating both forward and backward in the five layer system shown in Figure 22.

Layers one and five are the semiconductor material, layers two and four are the Alumina material, and layer three is the sample.

The two g planes are the (copper) thermal ground planes, plane a is where temperature is measured and plane d where heat is delivered to/removed from the system. At the interface of two layers, plane z, two boundary conditions must be satisfied as discussed in the Introduction:[21]

$$T_{fLz} + T_{bLz} = T_{fRz} + T_{bRz} \quad (5\text{-}12)$$

$$J_z = (J_{fRz} - J_{fLz}) + (J_{bRz} - J_{bL}) \quad (5\text{-}13)$$

$$\text{where} \quad J = -k dT/dx. \quad (5\text{-}14)$$

Here R = right, L = left, of the plane; f = forward (to the right), b = backward travelling waves.

Equation (5-12) holds at all planes, because each cross sectional plane is assumed to be at one uniform temperature. Equation (5-13) holds at all planes with $J_i = 0$, no internal heat sources, except at plane d where J_d is nonzero, since the driver Melcor is injecting/rejecting heat at plane d.

The expressions that relate the temperatures at the opposite ends of a layer of material as in Figure 23 are:

$$T_{f1a} e^{-(1+i)\phi_1} = T_{f1g} \quad (5\text{-}15a)$$

$$T_{b1a}e^{(1+i)\phi_1} = T_{b1g} \quad . \quad (5\text{-}15b)$$

These are the boundary temperature relations. The last subscript refers to the plane designated in Fig. 23, and the meaning of φ_1 is explained below.

At the rightmost plane g,

$T_{f1g} + T_{b1g} = 0$, then using the boundary temperature relations it can be shown that

$$T_{b1a} = -T_{f1a}e^{-2(1+i)\phi_1} \quad (5\text{-}16) .$$

Plane a is the junction between the alumina and semiconductor layers of the receiver Melcor and hence where temperature is measured.

The temperature boundary condition yields two expressions:

$$T_m = T_{f1a} + T_{b1a} = T_{f2a} + T_{b2a} \quad . \quad (5\text{-}17a,b)$$

Substituting in boundary temperature relations (5-16) and (5-17a) yields:

$$T_{f1a} = T_m/[1 - e^{-2(1+i)\phi_1}] \quad (5\text{-}18a)$$

$$T_{b1a} = -T_m/[e^{2(1+i)\phi_1} - 1] \quad (5\text{-}19b) \quad .$$

Now appling the heat flux boundary condition to plane a yields:

$$0 = (1+i)[n_1T_{f1a} - n_2T_{f2a} - n_1T_{b1a} + n_2T_{b2a}] \quad (5\text{-}20) \quad .$$

The general forms of n_i and φ_i are, $n_i = (\pi f C_i k_i)^{1/2}$ and $\varphi_i = w_i(\pi f C_i/k_i)^{1/2}$, where w_i is the thickness of sample material and f is frequency.

From relations (5-18) and boundary conditions (5-17b) and (5-20), expressions for T_{f2a} and T_{b2a} can be found.

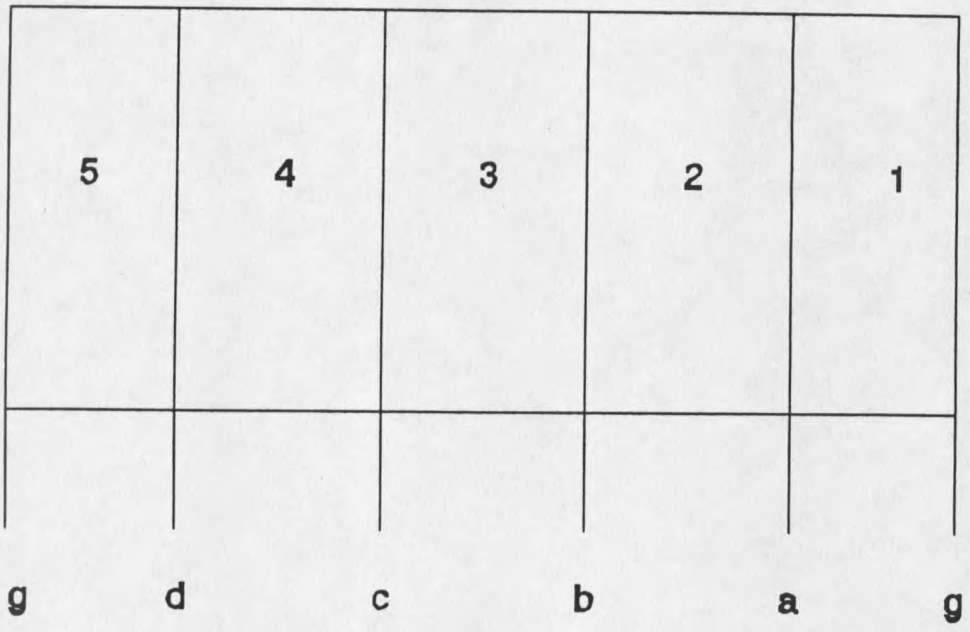

Five Layer System

Figure 22

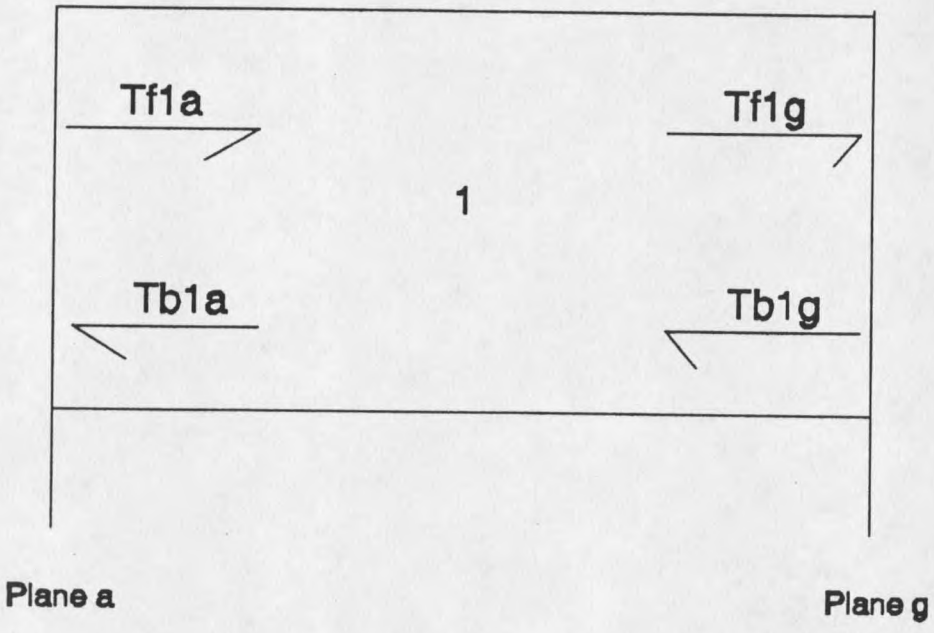

Bismuth Telluride

Figure 23

$$T_{f2a} = (T_m/2n_2)\{n_1/[1-e^{-2(1+i)\phi_1}] + n_1/[e^{2(1+i)\phi_1}-1] + n_2\} \quad (5\text{-}19)$$

$$T_{b2a} = (T_m/2n_2)\{n_2 - n_1/[e^{2(1+i)\phi_1}-1] - n_1/[1-e^{-2(1+i)\phi_1}]\} \quad (5\text{-}20) .$$

At plane b the first boundary condition is applied yielding

$$T_{f3b} + T_{b3b} = T_{f2b} + T_{b2b} \quad (5\text{-}20a)$$

then the boundary temperature relations yield $T_{f2b} = T_{f2a}e^{(1+i)\phi_2}$ and $T_{b2b} = T_{b2a}e^{-(1+i)\phi_2}$. Applying the second boundary condition yields:

$$n_2T_{f2b} - n_2T_{b2b} - n_3T_{f3b} + n_3T_{b3b} = 0 \quad (5\text{-}21) .$$

Now expressions for T_{f2b}, T_{b2b}, and (5-21) will yield:

$$T_{f3b} = [(n_2 + n_3)/2n_3]T_{f2b} + [(n_3 - n_2)/2n_3]T_{b2b} \quad (5\text{-}22)$$

$$T_{b3b} = [(n_2 + n_3)/2n_3]T_{b2b} + [(n_3 - n_2)/2n_3]T_{f2b} \quad (5\text{-}23) .$$

At plane c the previous series of steps yields expressions for T_{f4c} and T_{b4c}.

$$T_{f4c} = [(n_3 + n_4)/2n_4]T_{f3c} + [(n_4 - n_3)/2n_4]T_{b3c} \quad (5\text{-}24)$$

$$T_{b4c} = [(n_4 - n_3)/2n_4]T_{f3c} + [(n_4 + n_3)/2n_4]T_{b3c} \quad (5\text{-}25)$$

Now at plane d (Figure 26) the temperature T_2 is unknown, so the first boundary condition

$$T_{f5d} + T_{b5d} = T_{f4d} + T_{b4d} = T_2 \quad (5\text{-}26)$$

along with the propagation expressions and the second boundary condition yield:

$$J_d = (1+i)[n_5(T_{b5d} - T_{f5d}) + n_4(T_{f4d} - T_{b4d})], \quad (5\text{-}27)$$

where J_d is the heat current flux delivered to the system by the driver Melcor. Now, examining the left thermal ground plane, where the relation $T_{f5g} + T_{bfg} = 0$ at plane g along with the boundary temperature relations and the boundary conditions at plane d yield:

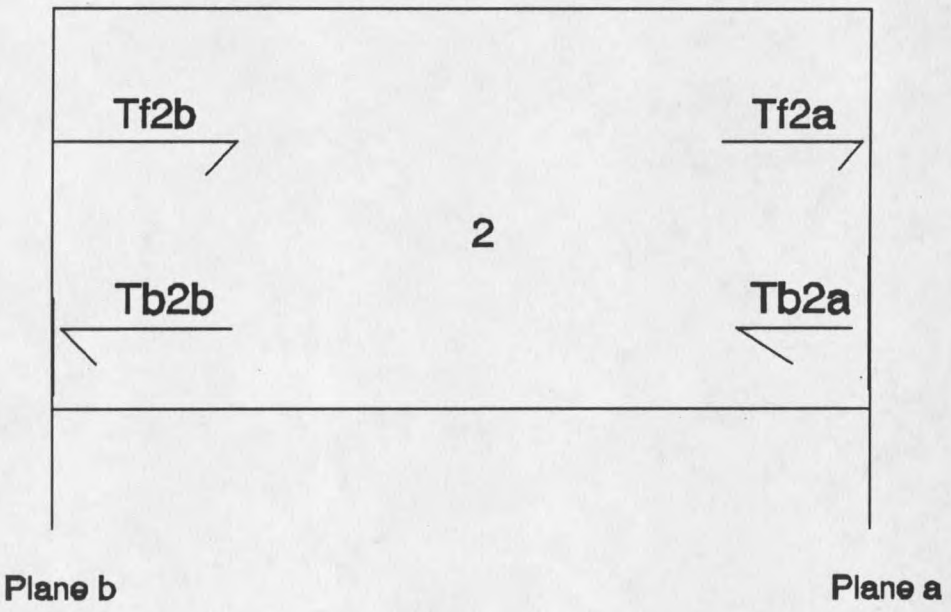

Alumina

Figure 24

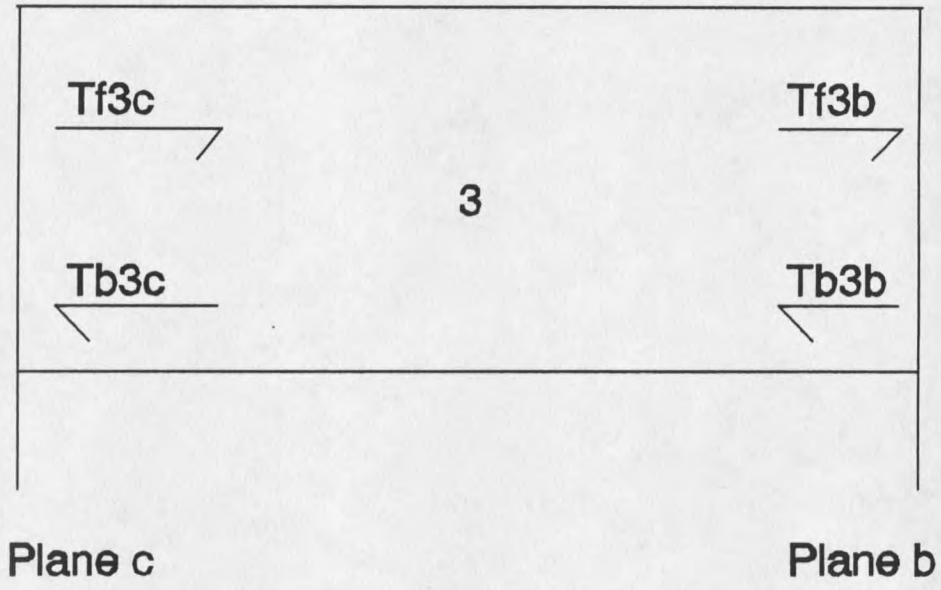

Sample Layer

Figure 25

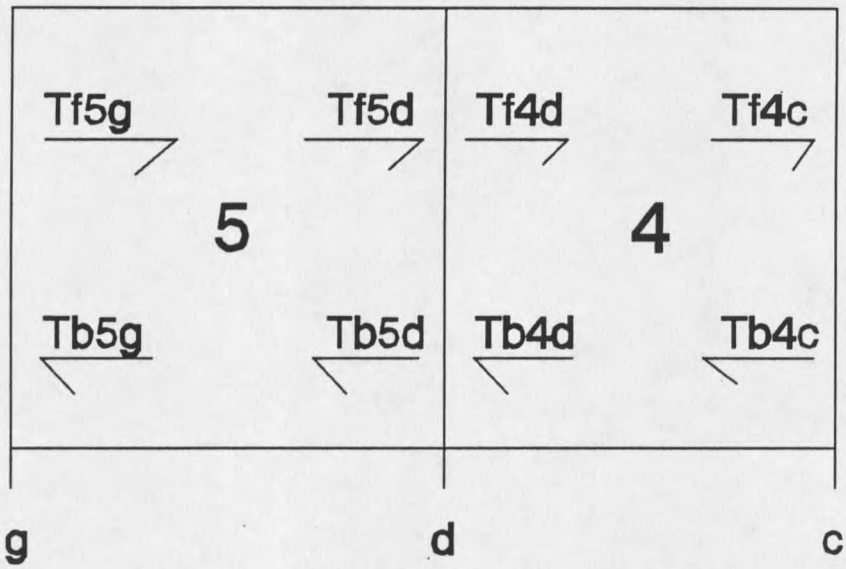

Bismuth Telluride and Alumina Layers

Figure 26

$$(T_{b5d}-T_{f5d}) = [(1+e^{-2(1+i)\phi_1})/(1-e^{-2(1+i)\phi_1})](T_{f4d}+T_{b4d}) \quad (5\text{-}28) \ .$$

Then the relation (5-27) becomes:

$$J_d = (1+i)\{n_1[(1+e^{-2(1+i)\phi_1})/(1-e^{-2(1+i)\phi_1})](T_{f4d}+T_{b4d}) + n_2(T_{f4d}-T_{b4d})\} \quad (5\text{-}29)$$

with $n_2=n_4$, $n_1=n_5$, $\phi_2=\phi_4$, and $\phi_1=\phi_5$. To find the heat current from the heat current flux, relation (5-29) is multiplied by an area A. Thus the expression for the heat current is:

$$H_d = (1+i)\{An_1[(1+e^{-2(1+i)\phi_1})/(1-e^{-2(1+i)\phi_1})](T_{f4d}+T_{b4d}) + An_2(T_{f4d}-T_{b4d})\} \quad (5\text{-}30) \ .$$

Since the data gathered in these experiments is simply the measured temperature T_m at plane a, actually gathered as voltage then converted to temperature, those values can be inserted into the above mathematical model in order to generate a value of heat current H_d, at plane d.

The value of the heat current injected/absorbed by the driver Melcor into/from the system is calculated directly by the relation $P_o = 0.502(\text{Watts/Amp})I_o$. This equation results from $|P_o| = (0.500)I_o \pm (0.281)I^2$ of the dc heat flow model. The quadratic term in the equation is dropped because the lock-in amplifier filters out any dc and double frequency components of the receiver Melcor output signal. Such signals would arise from the $(I_o)^2$ term since the trigonometric identity for $\sin^2\phi$ is $\sin^2\phi = 1/2 - (1/2)\cos 2\phi$.

Thus the result of (5-30) would then be compared to the result of $P_o = 0.502(W/A)I_o$ as a measure of the validity of the ac heat flow model.

The calculations begin with T_m at plane a and determine the temperature values at each plane back to plane d, the heat injection/absorption plane. The notation was simplified and the equations arranged in the sequence shown in Appendix A. The calculations were facilitated by use of an HP 48G programmable calculator which handles complex numbers readily.

In the course of working backwards from plane a to plane d, the properties of all three materials, bismuth telluride, alumina, and the sample, must be assigned values. For the bismuth telluride and alumina layers the accepted values of heat capacity per unit volume and thermal conductivity were assigned. The samples were assigned trial values of thermal conductivity and heat capacity, and these were adjusted to improve the overall fit of calculated to actual heat input over the whole frequency range.

For channel I, no sample was placed between the driver and receiver Melcors. This situation would be represented in the calculation by $\varphi_3 = 0$ and $n_3 = n_2 = n_4$. We obtained better results assuming a thickness of 0.01 mm of thermal grease.

Then, the equation $P_o = 0.502\,(W/A)\,I_o$ yields $J_{inm} = 23693 W/m^2 \angle 0°$, and (5-30) yields $J_{inp} = 17331 W/m^2 \angle -1.7°$ at 0.5 Hz which is lower than the J_{inm} value, but the phase angle error is small. Then at 1.5 Hz, $J_{inp} = 18343 W/m^2 \angle +3.3°$ which is an improvement. Finally at 15 Hz, $J_{inp} = 20518 W/m^2 \angle +53.9°$, so the predicted heat current has improved further but the phase

angle error has become large.

The calculated heat currents J_{inp} at each frequency for the no sample case are listed in Table 5, along with J_{inm}. Likewise, the calculated J_{inp} values for the lead sample are in Table 6, and for TGFB in Table 7.

Then to determine the predicted value of ,T , T_{mp} use, $T_{mp}J_{inp}\angle+\varphi_p = T_{mm}J_{inm}\angle+\varphi_m$ and solve for T_{mp},

$T_{mp} = T_{mm}(J_{inm}/J_{inp})\angle-\varphi_p + \varphi_m$.

The values of T_{mm} for the no sample, lead sample, and TGFB sample cases are in Tables 2, 3, and 4 respectively.

The values of T_{mp} are in Tables 8, 9, and 10 respectively.

Frequency	Input Heat Flux	Phase Angle
0.5 Hz	17,331 W/m^2	-1.7°
0.7 Hz	17,399 W/m^2	-1.0°
1.0 Hz	17,827 W/m^2	+1.7°
1.5 Hz	18,343 W/m^2	+3.3°
2.0 Hz	18,590 W/m^2	+4.8°
3.0 Hz	18,670 W/m^2	+8.0°
5.0 Hz	19,305 W/m^2	+16.1°
7.0 Hz	19,609 W/m^2	+23.5°
10.0 Hz	19,789 W/m^2	+34.1°
15.0 Hz	20,518 W/m^2	+53.9°

Calculated Input Heat Flux for No Sample

Table 5

Frequency	Input Heat Flux	Phase Angle
0.5 Hz	18,976 W/m^2	- 2.0°
0.7 Hz	18,991 W/m^2	- 1.0°
1.0 Hz	19,168 W/m^2	+ 1.8°
1.5 Hz	19,594 W/m^2	+ 3.8°
2.0 Hz	19,778 W/m^2	+ 7.2°
3.0 Hz	19,937 W/m^2	+11.0°
5.0 Hz	19,805 W/m^2	+21.7°
7.0 Hz	19,564 W/m^2	+31.6°
10.0 Hz	15,181 W/m^2	+35.1°
15.0 Hz	11,824 W/m^2	-16.2°

Calculated Input Heat Flux for Lead Sample

Table 6

Frequency	Input Heat Flux	Phase Angle
0.5 Hz	22932 W/m^2	- 6.6°
0.7 Hz	24792 W/m^2	- 2.8°
1.0 Hz	24366 W/m^2	+ 1.1°
1.5 Hz	23542 W/m^2	+ 6.1°
2.0 Hz	22606 W/m^2	+10.5°
3.0 Hz	20699 W/m^2	+18.9°

Calculated Input Heat Flux for TGFB Sample

Table 7

Frequency	Temperature	Phase Angle
0.5 Hz	1.034 K	-100.2°
0.7 Hz	0.722 K	-108.3°
1.0 Hz	0.482 K	-118.5°
1.5 Hz	0.293 K	-132.7°
2.0 Hz	0.199 K	-144.8°
3.0 Hz	0.108 K	-164.9°
5.0 Hz	0.0442 K	+164.5°
7.0 Hz	0.0227 K	+140.5°
10.0 Hz	0.0104 K	+110.3°
15.0 Hz	0.0038 K	+68.1°

Calculated Temperature for No Sample

Table 8

Frequency	Temperature	Phase Angle
0.5 Hz	0.926 K	-117.4°
0.7 Hz	0.6072 K	-129.9°
1.0 Hz	0.3689 K	-144.9°
1.5 Hz	0.1955 K	-163.8°
2.0 Hz	0.1194 K	-178.8°
3.0 Hz	0.0563 K	+157.3°
5.0 Hz	0.0196 K	+119.6°
7.0 Hz	0.0090 K	+ 87.9°
10.0 Hz	0.0036 K	+ 46.1°
15.0 Hz	0.00105 K	- 13.5°

Calculated Temperature for Lead Sample

Table 9

Frequency	Temperature	Phase Angle
0.5 Hz	0.10914 K	+163.9°
0.7 Hz	0.05403 K	+145.4°
1.0 Hz	0.02451 K	+122.7°
1.5 Hz	0.00922 K	+ 91.0°
2.0 Hz	0.00431 K	+ 63.9°
3.0 Hz	0.00131 K	+ 17.8°

Calculated Temperature for TGFB Sample

Table 10

CHAPTER 6

DATA ANALYSIS

The first step in the dc calibration of the probe was initially done without samples, the results of which are displayed in Figure 10.

The second step in the dc calibration was conducted while the lead and TGFB samples were in place in channels II and III respectively while channel I maintained no sample. The data gathered from this dc calibration was then used as the dc limit of the calculations and thus to determine the thermal conductivity of Lead and TGFB as discussed in chapter five. These data are plotted in Figure 11.

The next step in the development of the system as a measurement device was to apply known AC voltage signals to all three channels and observe the system response. This process was completed while the system was at room temperature. The results are displayed in Figures 16, 17, and 18.

The data displayed in Tables 2, 3, and 4, are the in-phase and quadrature voltages for six consecutive data runs for each of the three channels at each frequency. Before plotting, the voltage magnitude and phase angle of each run

were determined; then from these values the average voltage magnitude and average phase angle were determined. The average voltage magnitude was then converted into a temperature value by multiplying by the factor $0.63K/V(2)^{1/2}$ which was found from the Seebeck response of the Melcors, as described in Chapter 3. The average phase angle was adjusted by the proper amount corresponding to frequency as depicted in Table 1 in order to compensate for phase error of the in-phase and quadrature voltages at low frequencies. The plots of these values are shown in Figures 16, 17, and 18. Polar coordinates are used with the radial variable scaled logarithmically since there is a change of three orders of magnitude in temperature values over the frequency range 0.5 Hz to 15 Hz.

All three plots show the characteristic inward spiraling to the origin of the coordinate system as the frequency of the applied signal increases.

In the three cases the error bars on the temperature values are at best less than one percent of the temperature value and in the worst case, occurring at the higher frequencies, nearly ten percent of the corresponding temperature value.

In viewing the data in Tables 2, 3, and 4, it becomes clear that the accuracy of the in-phase and quadrature voltages is no better than ±0.0005 mV. This is due to some rounding-off occurring in the analog-to-digital conversion

of the in-phase and quadrature voltages from the lock-in amplifier to the data acquisition system. Likewise the error bars for the phase angles increase with increasing frequency, below or at one percent of the phase angle, then increasing to around ten percent at the highest frequencies.

The calculated and measured complex temperature values at the sensors are displayed in Figures 16-18. Since the calculations did not take any frequency dependence into account, and the calculated values show a good match to the data, it appears that no frequency dependence of the specific heat values exists for lead over the range 0.5 Hz to 30.0 Hz nor for TGFB over the same frequency range.

The final step in the development of this system was to gather data on TGFB over a temperature range which included the ferroelectric transition temperature of +75°C.[2] The overall response in going from +50°C to +80°C, then returning to +70°C, is shown in Figure 19.

The initial hope was to be able to observe the ferroelectric transition of TGFB which because of high heat capacity would be observed as a region of small temperature wave amplitude over the entire frequency range when the system was at +75°C.

In reviewing Figure 19, no significant deviation from the temperature wave pattern at other system temperatures was observed at the system temperature of +75°C. This is not to say that such observations are beyond the scope of the

apparatus, because further refinements to the design may make such observations possible.

CHAPTER 7

CONCLUSION

Upon completion of this project several conclusions are made regarding the performance of the present system with the resulting data, and improvements for future redesign of the system.

Current System Performance

In reviewing the performance of the apparatus and the resulting data, Figures 16 through 18 reveal good agreement for the no sample and lead sample cases over the frequency range 0.5 Hz to 15.0 Hz, and for the TGFB sample over the frequency range 0.5 Hz to 3.0 Hz. Further iteration of the T_{mp} and J_{inp} calculations show promise of acheiving better fit through more careful choices of k_x and C_x especially for TGFB. The values of k and C for TGFB which fit the data the best were k_{TGFB}= 0.28 W/m-K and C_{TGFB}= 1.333 x 10^6 J/m^3-K. For the case of the lead Sample C_{Pb}= 1.45 x 10^6 J/m^3-K , the accepted value, was used while k_{Pb}= 8.7 W/m-K worked best.

Future System Design

In review, several improvements to the future design of the apparatus become immediately obvious. A new lock-in amplifier which has an increased sub-hertz range along with GPIB compatibility is desirable. The sub-hertz capability of

a new lock-in would allow access to data in the frequency range 0 Hz(dc) to 0.5 Hz. These data points would begin as dc values along the real axis with zero phase angle and are clearly missing would fill in the large gaps evident in Figures 16 through 18.

The GPIB capability of a new lock-in would eliminate the need for the plotter which currently acts as an A/D board between the lock-in amplifier and the computer. Also the frequency locking signals would be sent directly to the computer, thus eliminating the need for manual observation of the process. Thus one could complete a data run at a given frequency, change the frequency, allow the system to lock on to the new frequency, and gather another run of data much more efficiently than before.

A second improvement would be to replace the present switch box which is manually operated with a GPIB compatible switch box. The device would make use of solid state relays which would be controlled by the computer in order to select which of the three channels data is to be gathered from.

Future redesign of the apparatus may or may not be able to improve the systems current vacuum capability. At this time it is unclear how important a role is played by establishing a good vacuum inside the apparatus in order to gain repeatable results.

Further improvements to the measurement process must include methods to enhance thermal contact between the

alumina surfaces of the Melcors and the solid samples. Such improvements would be heat sink compounds with a thermal conductivity greater than that which is currently used. As mentioned before, another possibility is polishing those surfaces which will be in thermal contact.

Currently the system is designed only for examining solid samples. Modifying the design to allow the study of liquid samples would certainly make the system more versatile.

In summary, it is clear that immediate upgrades to the current apparatus design are necessary in order to improve both the efficency of gathering data and its accuracy. Less clear is the possibility of finding a frequency dependency of specific heat values of various materials both solid and liquid.

REFERENCES

1. L. Marton, K. Lark-Horovitz, V.A. Johnson, "Methods of Experimental Physics Vol. 6 Parts A and B" Academic Press, New York, 1959.

2. F. Jona, G. Shirane, "Ferroelectric Crystals" MacMillan, New York, 1962.

3. D. D. Pollock, "Thermocouples Theory and Properties" CRC Press, Ann Arbor, 1991.

4. P.F. Sullivan, G. Seidel, Phys. Rev. 173, 679 1968.

5. N. Savvides, W. Murray, J. Phys. E: Sci. Instrum. 11, 941 1978.

6. P.Handler,D.E. Mapother, and M. Rayl, Phys. Rev. Lett. 19, 356 (1967).

7. K.M. Cheung and F.G. Ullman, Phys. Rev. B 10,4760 (1974).

8. G. Yang, A.D. Migone, and K.W. Johnson, Phys. Rev. B 45, 157 (1992).

9. A. Santucci, L. Verdini, Rev. Sci. Instrum. 57, 1627 1986.

10. M.L. Stanley, A.D. Reich, U.S. Patent 3,733,887 1973.

11. MELCOR, Materials Electronic Products Corporation, 990 Spruce Street, Trenton, New Jersey 08648.

12. V.H. Schmidt, private communication.

13. Technical discussions with, and assistance from, Mr. Erik Andersen.

14. N.D. Ashcroft and N.M. Mermin, "Solid State Physics" Holt Rinehart and Winston, Philadelphia, 1976.

15. EG&G Technical Papers, EG&G Princton Applied Research, Princeton, New Jersey 08543-2565.

16. Technical discussions with, and assistance from, Mr. Norman Williams.

REFERENCES-CONTINUED

17. Technical discussions with, and assistance from, Mr. Robert Parker.

18. Helmut Wolf, "Heat Transfer" Harper & Row, New York, 1983.

19. Dow Corning Technical Papers, Dow Corning Corporation, Midland, Michigan 48686-0994.

20. T.T. Wang, J.M. Herbert, A.M. Glass, "The Applications of Ferroelectric Polymers" Blackie, Glasgow, 1988.

21. A.L. Fetter, J.D. Walecka, "Theoretical Mechanics of Particles and Continua" McGraw-Hill, New York, 1980.

APPENDIX

Equations used in ac heat flow calculations of chapter five:

1. $T_{f1a} = T_m/(1 - \exp[-2(1+i)\varphi_1]) \equiv T_{f1g}$
2. $T_{b1a} = -T_m/(\exp[2(1+i)\varphi_1] - 1) \equiv T_{b1g}$
3. $T_{f2a} = n_{21+}T_{f1a} + n_{21-}T_{b1a} \equiv T_{f2r}$

   where $n_{ij\pm} = (n_i \pm n_j)/2n_i$
4. $T_{b2a} = n_{21-}T_{f1a} + n_{21+}T_{b1a} \equiv T_{b2r}$
5. $T_{f2b} = T_{f2a}\exp[(1+i)\varphi_2] \equiv T_{f2g}$
6. $T_{b2b} = T_{b2a}\exp[-(1+i)\varphi_2] \equiv T_{b2g}$
7. $T_{f3b} \equiv T_{f3r} = n_{32+}T_{f2g} + n_{32-}T_{b2g}$
8. $T_{b3r} = n_{32-}T_{f2g} + n_{32+}T_{b2g}$
9. $T_{f3g} = T_{f3r}\exp[(1+i)\varphi_3]$
10. $T_{b3g} = T_{b3r}\exp[-(1+i)\varphi_3]$
11. $T_{f4r} = n_{43+}T_{f3g} + n_{43-}T_{b3g}$
12. $T_{b4r} = n_{43-}T_{f3g} + n_{43+}T_{b3g}$
13. $T_{f4g} = T_{f4r}\exp[(1+i)\varphi_4]$
14. $T_{b4g} = T_{b4r}\exp[(1+i)\varphi_4]$
15. $T_s = T_{f4g} + T_{b4g}$
16. $T_{f5r} = -T_s/(\exp[2(1+i)\varphi_5] - 1)$
17. $T_{b5r} = T_s/(1 - \exp[-2(1+i)\varphi_5])$
18. $J_{in} = (1+i)[\, n_5(T_{b5r} - T_{f5r}) + n_4(T_{f4g} - T_{b4g})\,]$